Electrochemical Affinity Sensors Using Field Effect Transducer Devices for Chemical Analysis

Hamdi Ben Halima, Abdelhamid Errachid, Nicole Jaffrezic-Renault

Electrochemical Affinity Sensors Using Field Effect Transducer Devices for Chemical Analysis

Hamdi Ben Halima, Abdelhamid Errachid, Nicole Jaffrezic-Renault*

University of Lyon, Institute of Analytical Sciences, 69100 Villeurbanne, France

*Corresponding author: Nicole Jaffrezic-Renault, e-mail address: nicole.jaffrezic@univ-lyon1.fr

Abstract

The review presents advances and main challenges of the affinity sensors based on field-effect transistors published during the last five years. The different nanomaterial-based field-effect transistors are classified according to the nature of the nanomaterials, beginning by silicon, the "gold-standard" semiconductor, the gallium nitride semiconductor, the organic semiconductors, the silicon nanowires, the inorganic nanomaterials, the carbon nanotubes and the graphene. Due to its exceptional electrical properties, the main works are devoted to graphene. The obtained analytical performances for the detection of biomarkers, of DNA sequences and of miRNA are listed. The relation between the operational conditions - nature of the nanomaterials, procedure of preparation, choice of the receptor molecule, method of immobilization – and the analytical performance are discussed. The perspective of industrialization of these affinity sensors based on field-effect transistors is discussed.

Keywords: FETs, silicon, graphene, silicon nanowires, carbon nanotubes, antibody, DNA

Introduction

Biosensors are defined as analytical devices used for the detection of a chemical substance, that combines a biological component with a transducer. Immunosensors are based on the immobilization of a specific antibody, a glycoprotein produced by the immune system to neutralyze foreign substances (antigens) to the body. The antibody is then able to identify and bind to antigens with an extremely high specificity. The immunosensor is able to detect the formation of the antigen-antibody complex through the modification of the transducer signal : electrochemical, optical, gravimetric, thermal…, without any labelling then leading to a simplified immunosensing procedure and a fast response time.

Aptamers consist of artificial oligonucleotide sequences (peptides or nucleic acids) which can recognize and bind to a wide range of targets ; they have drawn much attention as promising alternatives to conventional antibodies. Aptamers are produced through the *in vitro* selection and amplification of populations of random sequence oligonucleotide libraries, known as the SELEX process (selection evolution of ligands by exponential

enrichment). When specific sequences are identified, aptasensors can then replace immunosensors. Affinity sensors include immunosensors, aptasensors for the detection of chemical substances such as biomarkers, toxins … and nucleic acid sensors for the detection of DNA or RNA sequences.

Among various electrochemical transducers, those based on field-effect transistors (FETs) have attracted considerable attention because of their potential for miniaturization, multi sensing, fast response time and integration with electronic manufacturing processes, such as complementary metal-oxide semiconductors (CMOS). The concept of an ion-sensitive FET (ISFET) was introduced Bergveld [1] in the early 1970s; it was derived from a metal-oxide-semiconductor FET (MOSFET), when the metal gate was replaced by a reference electrode. For the detection of different target analytes, it results in a myriad of different sensor system combinations. The affinity sensors based on ISFET can be presented along the generic structure illustrated in Fig.1. The information obtained from the sample corresponds to the concentration/activity of the target analyte, which is transduced to an electrical signal via the field effect. Then, the signal can be amplified, processed, and displayed depending on the application.

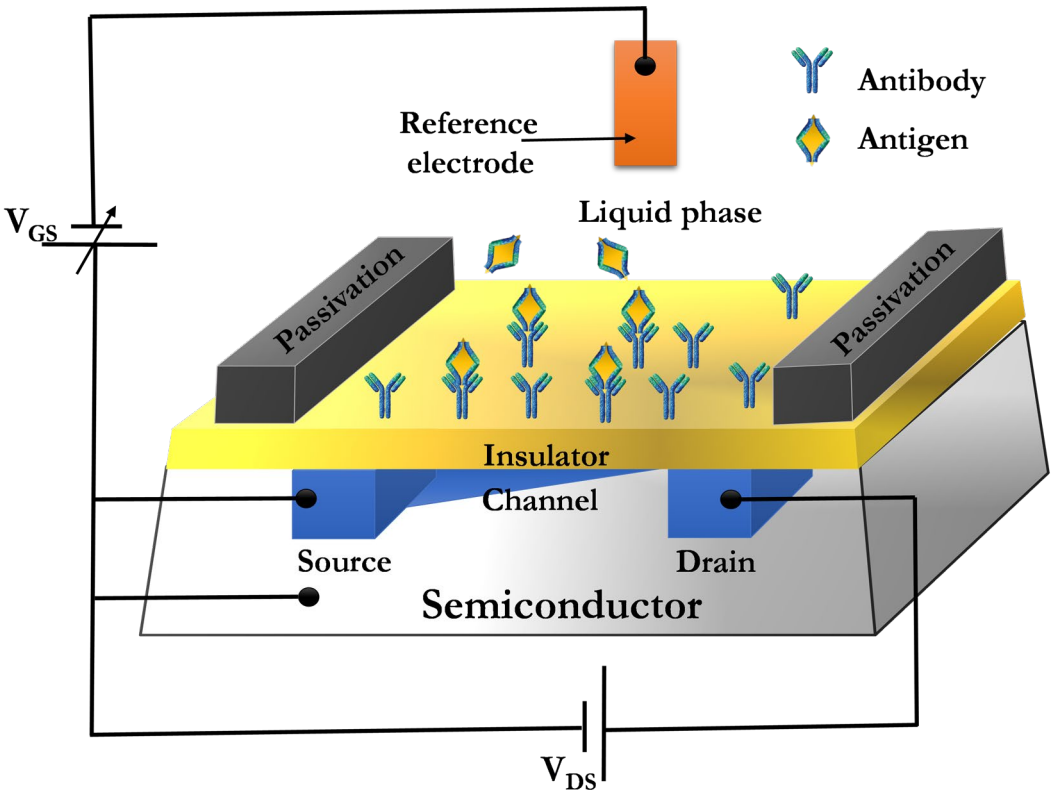

Figure 1. Generic structure of an affinity sensor based on a semiconductor field-effect transistor

A simplified potential diagram at the different interfaces of an affinity sensor based on a semiconductor field-effect transistor is shown in Fig. 2. The observed responses originate from the charge σ_0 resting at the sensing surface (the insulator surface grafted with the

receptor molecule). This charge sees capacitances on both sides : the capacitance is presented as a series combination of the double-layer and sensor (i.e., FET) capacitances, respectively, C_{DL} and C_{FET}, where C_{FET} comprises the insulator, C_{IN}, and channel, C_C, capacitances. The potential change at the sensing surface can be approximated by:

$$\psi_o = \Delta\sigma_o/(C_{DL} + C_{FET}) \qquad (1)$$

Depending on the transistor biasing, one or another capacitance can dominate. In weak inversion (low density of carriers in the channel), C_C will clearly be smaller and determine the overall sensor capacitance, in contrast to strong inversion (high density of carriers in the channel), where C_C can be omitted and C_{IN} is relevant. In all cases, these capacitances are usually clearly smaller than the double-layer capacitance. Hence, we can conclude that the transistor capacitance has a negligible effect on the sensitivity at the sensing interface.

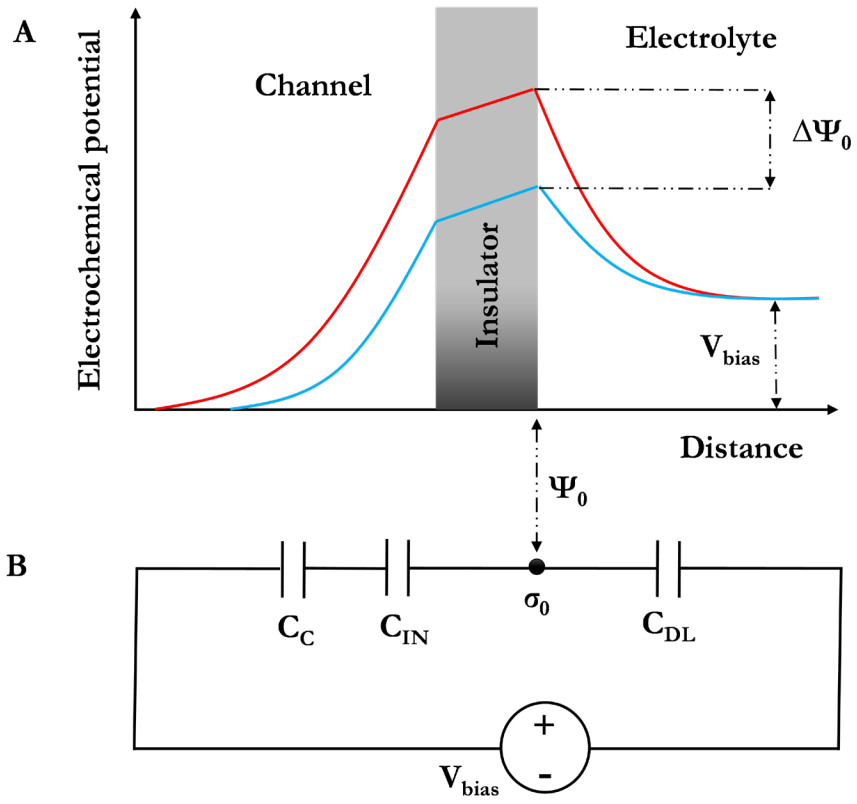

Fig. 2. A) Potential over a simplified model of electrochemical cell with an insulator as the interfacial material. The charge binding in the surface creates a potential shift, denoted by ΔΨ0, at the interface. B) Equivalent circuit model of the sensor where C_{DL}, C_{IN}, C_C are the double-layer, gate insulator, and channel capacitances, respectively. The interfacial charge, σ0, is surrounded by capacitors on both sides.

First, the charge at the sensing surface alters the insulator electric field, changing the potential at the outer surface of the electrode. Second, this potential shift subsequently alters the semiconductor drain current which is the transconductance effect of a FET.

A widely debated issue is the label-free detection of biomolecules using FET based biosensors. Originally, it was believed that the fact of biomolecules carrying intrinsic charge allowed their detection using field-effect devices. Despite significant efforts, the results were not satisfactory due to the electrical double layer. For instance, in ionic solutions, the small ions, which carry an opposite charge to that of the detectable large macromolecule, screen the observed net charge by a cloud of opposite charge around the macromolecules. Screening is dependent on the distance between the surface and the point of observation. The amount of observed charge is characterized by the Debye screening length. At a distance of one Debye length, the electrical signal decays to 1/e of its original value. Typical screening lengths are in the order of 1 nm, unless very diluted solutions are considered. This is considered to be the main reason limiting the label-free biosensor development. Fig. 3 depicts the electrical double-layer length compared to the size of several biomolecules; the larger the molecule, the stronger the screening effect. Additionally, linking the capture molecule to the surface commonly requires some linker molecules that further increase the distance to the target molecule [2].

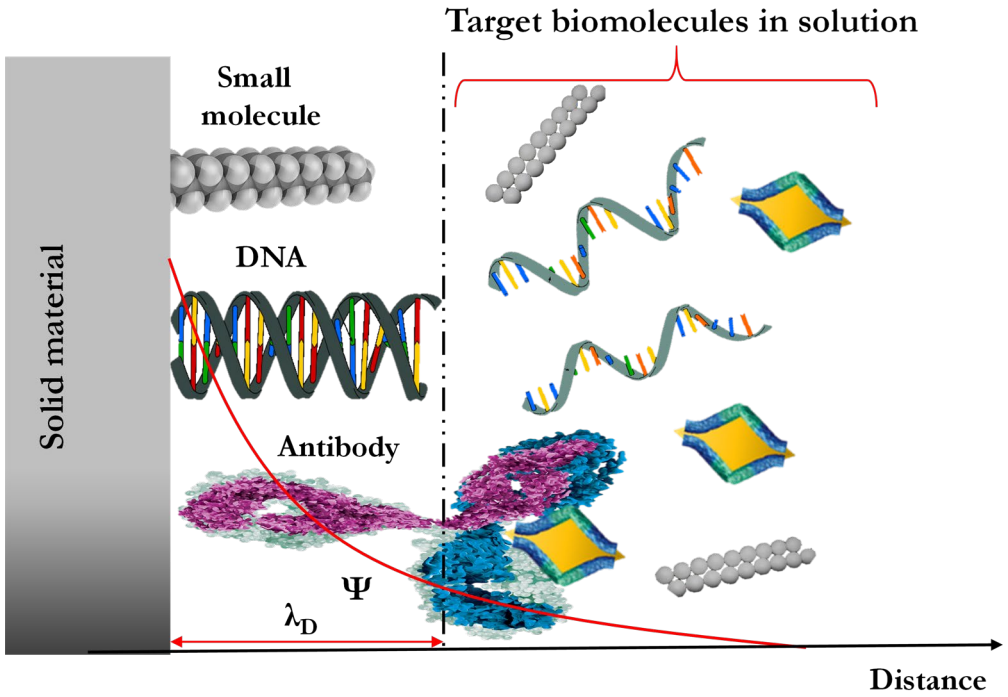

Fig. 3. Electrical double-layer length in the presence of different targets (dimensions are not scaled).

However, several reports claim successful label-free detection even in cases where the size of the complex, such as an antibody–antigen complex, is at vastly longer distances than the electric double layer. A common explanation for these observed results is the Donnan effect. According to this theory, proteins are considered as a membrane on the electrode surface. In addition, small ions can shuffle between the solution and this protein membrane. Then, when a fixed charge is present due to the target, a difference of ion concentration appears on the interface between the membrane and the solution. This redistribution of ions creates a detectable change in the interfacial potential. Moreover, the change in this Donnan potential also causes a shift in pH. Thus, the total response is the combination of the surface pH response and the Donnan potential.

During years 2020 and 2021, due to the COVID-19 epidemic period, a lot of review papers about biosensors for the detection of virus were published [3-14]. Among the cited affinity biosensors, FET based biosensors were cited, the most cited one being from Seo et al [3]. Other recent reviews were devoted to biosensors for the diagnostics of other health deficiencies and among them FET based affinity biosensors: chronic obstructive pulmonary disease [15], immunodeficiency [16], neurodegenerative diseases [17], diabetes mellitus [18,19], cardiac failure [20], acute ischemic stroke [21], cancer [22-24] and different pathologies [25]. Two recent reviews were devoted to biosensors for the detection of contaminants in environmental matrices such as pesticides/herbicides [26] and pharmaceuticals and endocrine-disrupting compounds [27].

Reviews about micro and nanoscale biosensors reported some FET devices. Some are based on graphene [28,29] or on self-assembled monolayers [30,31], or on AlGaN/GaN heterostructures [32], or on nanowires [33], or on nanotechnologies [3] or on molecularly imprinted polymers [35].

Since 2015, 14 reviews were devoted to field-effect transistors for biodetection. They were all oriented towards one type of field effect transistor: CMOS-type FETs [2,36], conductive polymer-based FETs [37-40], carbon nanotube-based FETs [41], graphene-based FETs [42-44], nanowire-based FETs [45], nanomaterial-based FETs [46-48].

This review is an exhaustive description of the works reported since 2015, on affinity sensors based on field effect transistors, whatever the nature of the nanomaterial-based FETs (silicon, graphene, SWCNTs, Si nanowires, organic FET, nanomaterials, GaN). The objective of this review is to study the relation between the analytical performance and the characteristics of the FETs (materials, structure and working parameters).

Silicon-based field-effect transistors for affinity sensing (Table 1)

Since 2015, only twelve papers were published in this field (Table 1). Seven of them are conventional ISFETs, they were devoted to the detection of biomarkers : lung cancer [49], asthma [50], mental stress [52], oxidative and nitrosative stress [53], heart failure [54], [55] and to the detection of virus [51].

They were fabricated through CMOS technology, the biofunctionalization being performed afterwards. The receptor molecule (antibody, amino modified aptamer or) was directly covalently grafted on the insulator surface (SiO_2 or Si_3N_4) through its silanization. In Refs 49 and 51, several FETs were fabricated on the same chip, then allowing the multidetection. Variation of the gate-source voltage was the measured signal, depending on the concentration of the biomarker. In Ref 6, impedance of the channel was measured, leading to a lower detection limit of TNF-α and a larger dynamic range, compared to the results obtained by measuring the variation of the gate-source voltage [53]. When the frequency is high enough, the ions in the solution are unable to form the double layer after the AC perturbations. This allows probing further into the solution, and it also decreases the sensitivity towards small absorbates within the double layer [2]. ALP-labeled secondary antibody was used in Ref 50 and low-cost electrical ELISA test that presents the same detection limit.), the obtained ISFET-based system becomes then a portable

Extended gate (EG) field-effect transistors were presented in six papers. This configuration allows is an improvement for passivation and packaging compared to the conventional ISFET. As shown in Fig. 4, the EG immunoFET consists of two parts: the gate of a MOSFET is connected to the extended gate. This one is an electrode modified with the receptor molecule (antibody), in contact with the solution. The MOSFET can be commercially available one, well packaged, avoiding any damage from humidify and no influence of the light. For the five published papers, the electrode used was a gold electrode.

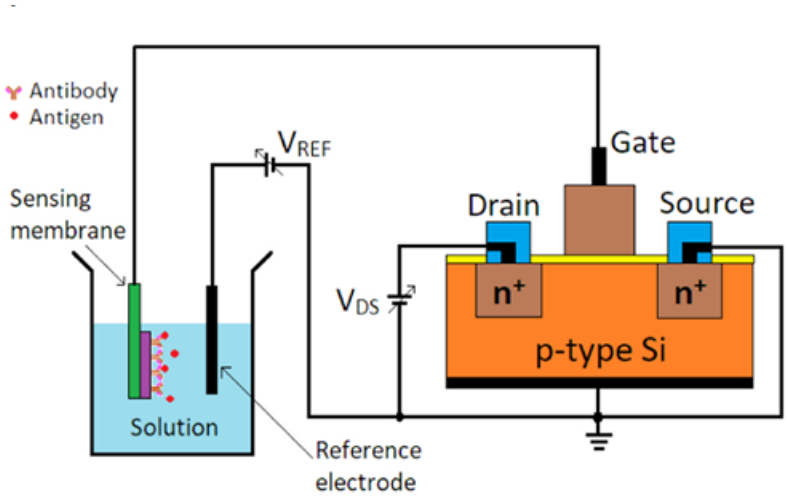

Figure 4. General scheme of an extended gate immunoFET

The presented EG-FET allows the detection of different biomarkers: thyroid carcinoma [57], breast cancer [58], Alzheimer disease [59], bacterial infection [60]. For the detection of DNA [56], PNA probes were used for the efficient hybridization in low salt conditions, which is required to limit the ion screening effect.

In Ref 60, an enhanced electric-double-layer (EnEDL) field-effect-transistor-based immunosensor was built (Fig. 5), for the successful detection of proteins in high ionic strength solutions. The results show that, as the EDL is enhanced at higher gate voltage or higher salt concentration, the sensitivity of detection increases. A detection limit of 0.5 mg of C-RP was obtained in whole blood and in PBS, without any dilution step.

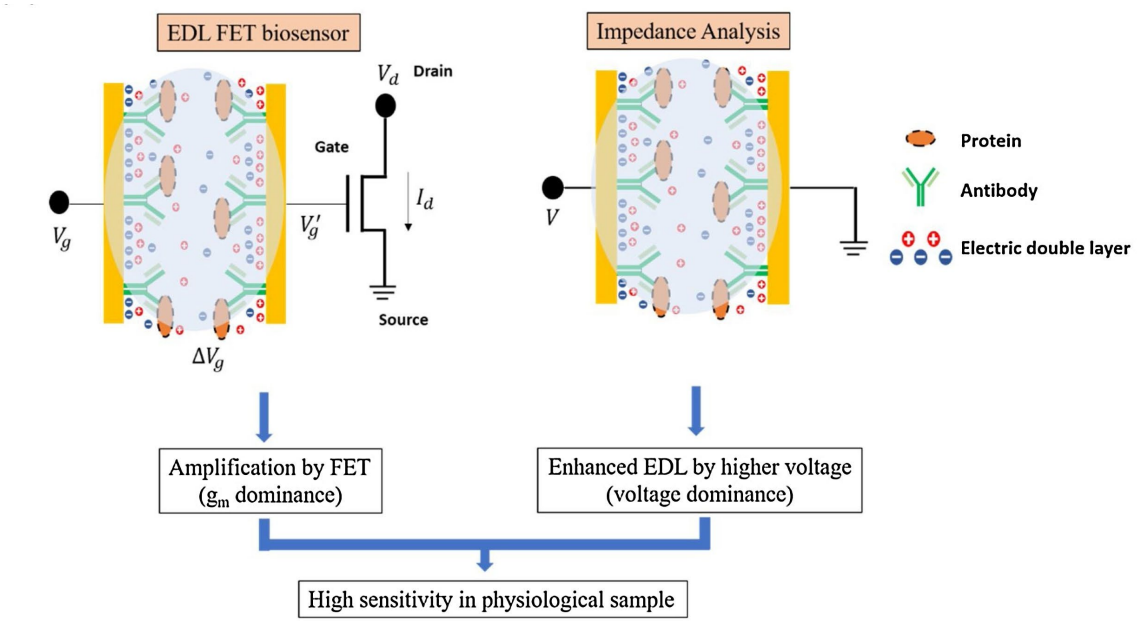

Figure 5. Scheme of enhanced electric-double-layer (EnEDL) field-effect transistor and impedance analysis. From [60]

AlGaN/GaN High Electron Mobility Transistors for affinity sensing (Table 2)

Compared to silicon-based field effect transistors, GaN based high electron mobility transistors (HEMT) present several advantages for affinity sensing:

- an exceptional chemical and physical stability of GaN allowing its use in liquid media without passivation
- a very high two-dimensional electron gas (2DEG), due to high polarization in AlGaN/GaN heterostructures (Fig. 6), results in high sensitivity
- environment friendly and bio-friendly with non-toxic surface content, GaN performs well for interaction with biological species

- GaN-based sensor does not need surface passivation and the, has instantaneously response to polar molecules.

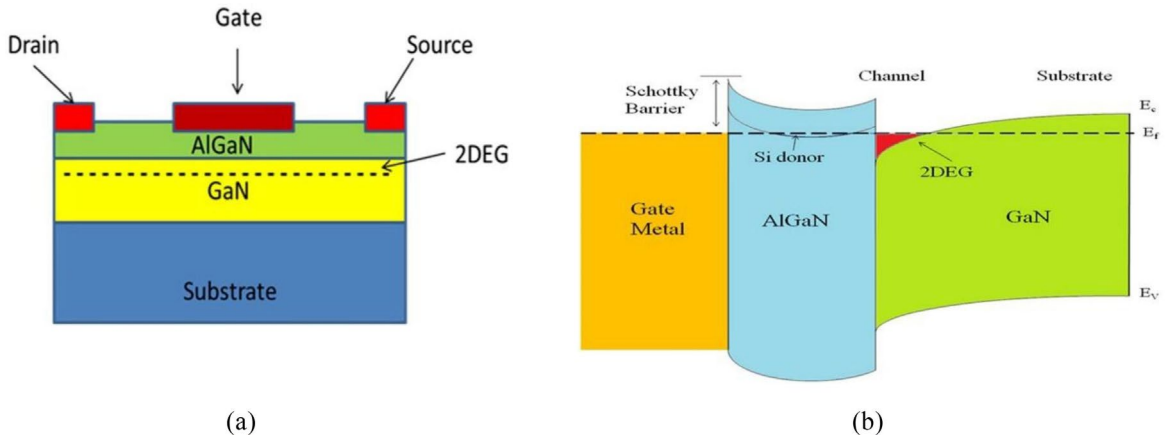

Figure 6. (a) Scheme of a AlGaN/GaN High Electron Mobility Transistor. (b) Energy band diagram. From [32]

Since 2015, nine papers were published on AlGaN/GaN HEMT for the detection of biomarkers of different diseases: bacterial infection [61], Zika virus [64], prostate cancer [65], [69], heart failure [66], mental stress [68] and DNA [62].

In Refs 63, 64 and 66, electric-double-Layer HEMT were fabricated, in order to defeat the severe charge-screening effect caused by high ionic strength in solution. The antibodies or the aptamers were grafted on the gold electrodes as well as in Ref 65 where the authors used a disposable extended gate. In order to enlarge the sensing capacity beyond the Debye-screening limit, Wang et al [69] used magnetic beads for the immobilization of the antibody and an electronic ELISA test was then built for PSA detection. A detection limit was of 1fg/mL was obtained which is one hundred times lower than that obtained with the extended gate HEMT [65]. A sensitive detection of cortisol (detection limit 1 pM) was obtained by the generation of a photocurrent through laser illumination of the HEMT sensor [68]).

Organic Field effect transistors for affinity sensing (Table 3)

The organic field effect transistor (OFET) structure resembles the basic silicon-based field-effect transistors, where silicon is replaced by an organic semiconductor (OSC) where the gate is biaised through the substrate for back-gated OFETs (Fig. 7a). Another configuration is the electrolyte-gated OFET (EGOFET) in which the gate is applied to the electrolyte (Fig. 7b). The recognition molecule (mainly antibody or ss-DNA) is immobilized on top of the OSC layer. Some OFETs with an extended gate (EG) allows the immobilization of the receptor molecule on the extended gate, as presented in Fig. 8. Several works published since 2015 were based on EG-OFETs [71], [74], [75], [81]. Different types of organic semiconductors were recently used: P3HT (poly-3-hexylthiophenepentacene [70], [72], [73], PBTTT (poly(2,5-bis(3-hexadecylthiophene-2-yl)thieno[3,2-*b*]thiophene) [71], pentancene [74], [75], TIPS-pentacene (6,13-bis(triisopropylsilylethinyl)pentacene) [76], [77], poly(DPP-DTT) (poly(N-

alkyldiketopyrrole dithienylthienol[3,2-*b*]thiophene) [78], PDVT-8 [79], diF-TES—ADT (2,8-difluoro-5,11-bis(triethylsilylethynyl)anthradithiophene) [80], PANI [81].

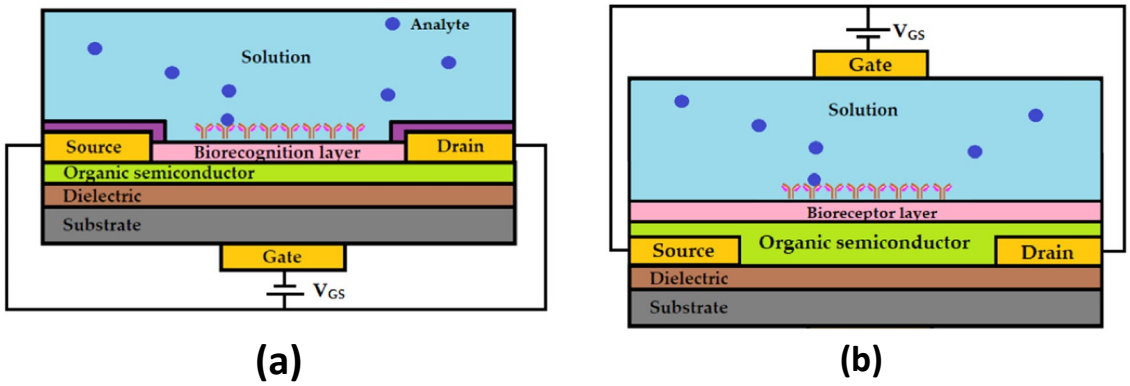

Figure 7. (a) Schematic representation of an organic FET (back gated). (b) Schematic representation of an electrolyte-gated organic FET structure. From [36]

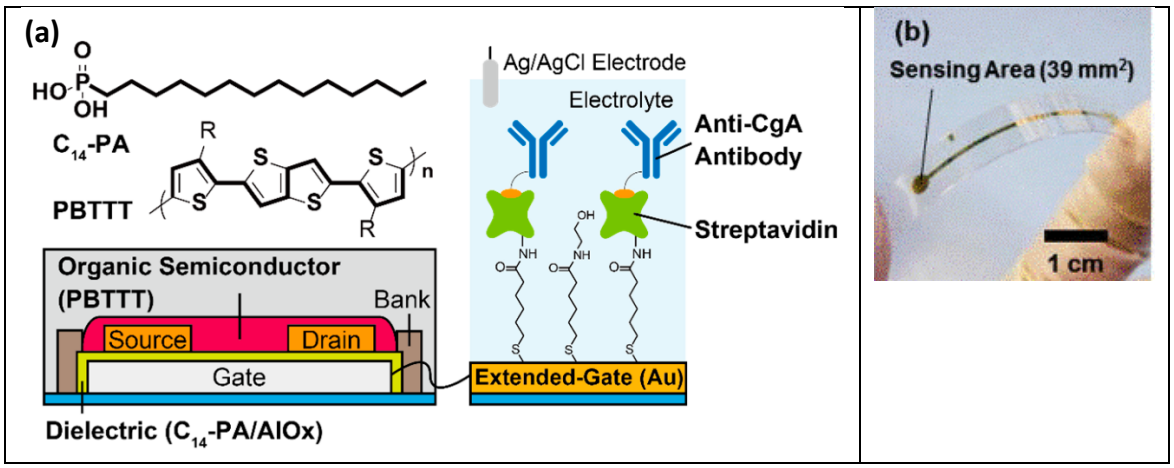

Figure 8. (a) Schematic structure of the designed extended-gate type OFET. (b) A photograph of the sensing portion (i.e. extended gate). From [71,82]

Since 2015 there were twelve papers published on OFET based affinity sensors for the detection of biomarkers of different diseases: bacterial infection [70], [72], endocrine tumors [71], sepsis [73], brain injuries [74], mental stress [75], [76], immune response against drugs [77], liver cancer [79], rheumatoid arthritis [80], rectal colon cancer [81]. One EGOFET based on immobilized algea in an hydrogel allows the detection of herbicides [78].

Several of these OFET-based affinity sensors were able to detect the biomarkers with a higher sensitivity, even in high ionic strength media such as serum. To increase the Debye screening length beyond bioanalyte/bioreceptor complex dimensions, a phospholipid layer [70], a polyethylene glycol (MW 5000) layer [74] or a poly(styrene-co-methacrylic acid)

(PSMA) layer [75] were used to change the properties in aqueous solution and then to increase the "effective Debye screening length", by keeping a low ion density environment for the binding protein. A larger drain current could then be obtained. When cortisol was detected in buffer, the antibody being embedded in PSMA, a detection limit of 1pg/mL, corresponding to 2.75 pM was obtained [75], while with an EGOFET functionalized with an aptamer, a detection limit of 27.3 pM was obtained [76], showing the interest of the Debye screening layer.

Silicon nanowire field-effect transistors for affinity sensing (Table 4)

The diameters on nanowires are comparable to the size scale of many biological species, such as proteins, nucleic acids. The nanowires (NW) configured as FETs have been used as sensitive real-time electricity –based detectors of biological species [33]. As "gold standard semiconductor", silicon presents high mobility carriers (100-1500 $cm^2/V/s$). silicon nanowires can be fabricated through a top-down approach based on CMOS fabrication process or through a bottom-up approach based on vapor-liquid-solid (VLS) growth mechanism where a metal nanocluster catalyst is used to direct the material growth along one direction.

The typical structure of a silicon nanowire FET, in liquid gated configuration, is presented in Fig. XX. As shown in this figure, at a constant source-drain voltage, the conductance of the SiNW change in response to the binding of biological species, depending of the own charge and depending on the doping of the nanowire. The sensitivity of the nanowire is critically dependent of its diameter, the higher sensitivity for smaller diameters is due to the larger surface/volume ratio. In addition, lower NW doping densities results in higher sensitivity [33]. For SiNW FET, the native oxide on the NW surface serves as gate oxide (Fig. 9) and the thinner the oxide, the higher the sensitivity.

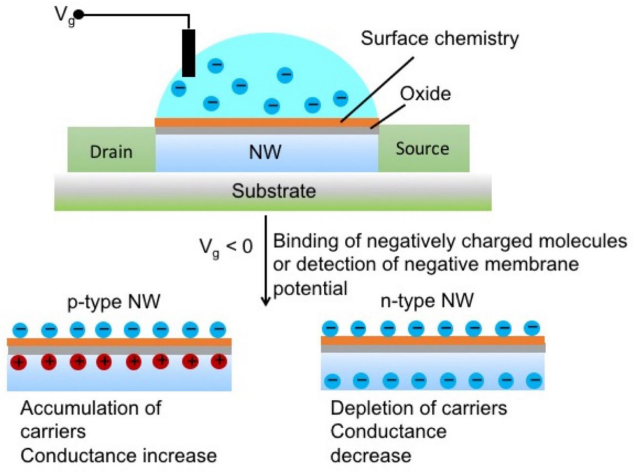

Figure 9. Scheme of a silicon nanowire field-effect transistor. From [33]

Since 2015, twelve papers were published on SiNW FET for the detection of biomarkers for different diseases (Table 4): bladder cancer [83], oral cancer [84], lung cancer [85], [87], prostate cancer [86], neurological disorder [88], heart disease [89], [90], parasitic infections [91], [93], Alzheimer disease [92], influenza [94]. Except one paper that presents a bottom-up approach for the VLS-CVD preparation of Si NWs [90], in the other papers, Si NWs were prepared through a top-down approach in a CMOS technology. All these biomarkers were detected in diluted ionic media, except in two papers where the detection was carried out in high-ionic strength environment. In Ref 90, the chemically-controlled antigen-dissociation detection approach was applied. A suitable "chemical environment" (addition of ethyleneglycol) which enabled the clear-up splitting of the dissociation regime window into two sub-regimes, was created, thus allowing the complete washing of the nonspecifically adsorbed salts and biomolecules, while significantly delaying the dissociation of the specific antigen-antibody pairs on the Si NW surface. It was then demonstrated the direct and quantitative detection of protein biomarkers (cTnT and cTnI), down to concentrations in the fM range, from unprocessed whole minuscule samples of only a few microliters.

A modification of a Si NW surface with a porous and biomolecule-permeable polymer layer (PEG) was used to increase the effective Debye screening length and then the sensitivity of detection [93]. The different scheme of the modified Si NW surface is presented in Fig. 10. In a first step the replacement of the whole anti-IgG antibody (Wab) and by a reduced anti-IgG antibody (Fab) improves the sensitivity of detection after amplification by the R18 aptamer (Fig. 10A). The Fab/PEG-SiNWFET immunosensor exhibited the lower detection limit of 1 pg/mL, not achievable with the other configurations of SiNW FET interface (Fig. 10B).

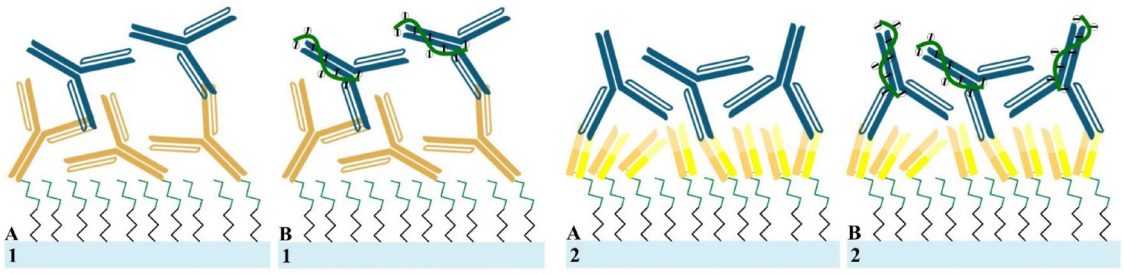

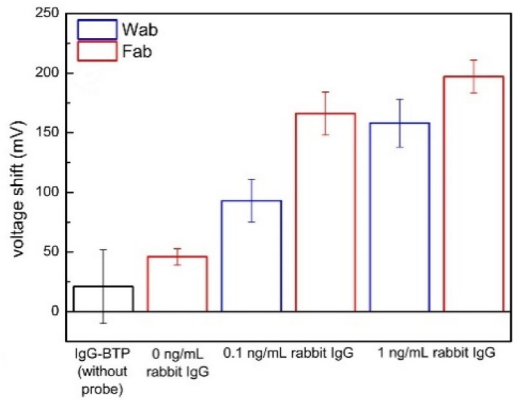

(A)

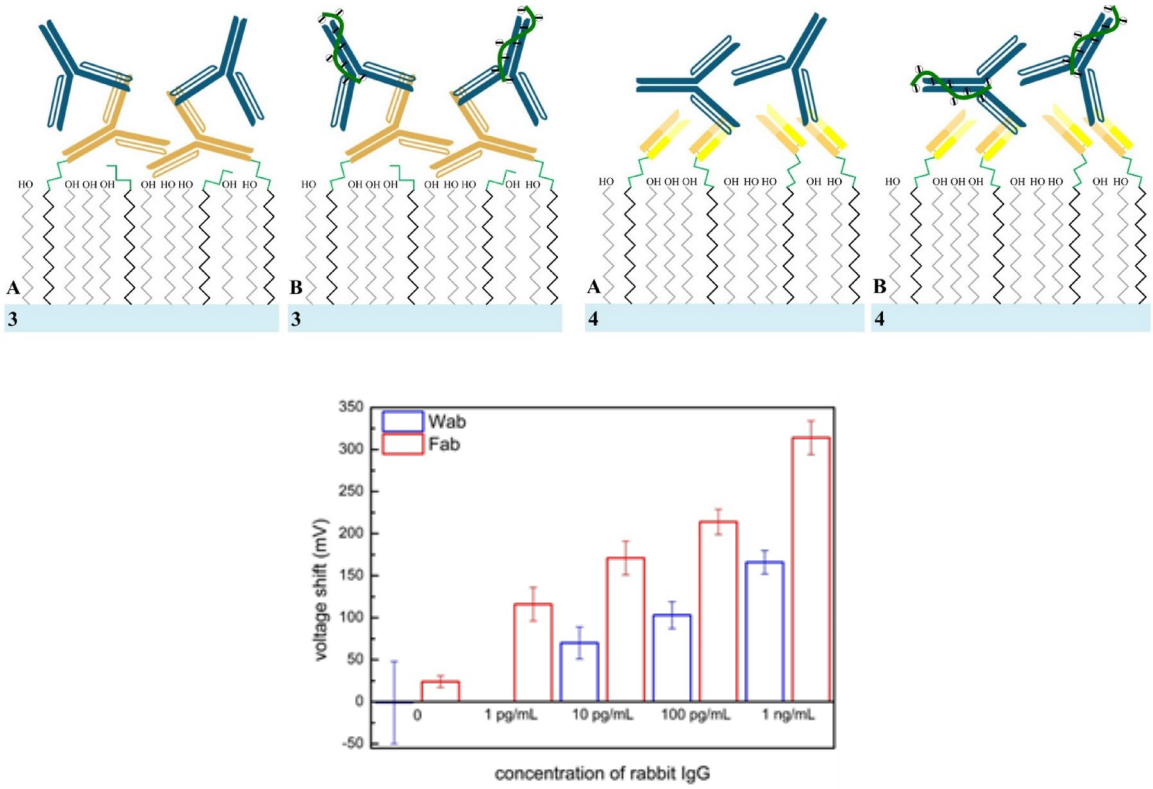

(B)

Figure 10. (A) Illustration of the detection of rabbit IgG by (1) Wab/APTES-SiNWFETs, (2) Fab/APTES-SiNWFETs, as well as their corresponding signal enhancement by R18 aptamer in this study. Voltage shift in presence 0 ng/ml, 0.1 ng/mL, and 1 ng/mL of rabbit IgG, in 150 mM BTP (Bis-Tris propane). (B) Illustration of the detection of rabbit IgG by (3) Wab/PEG-SiNWFETs, and (4) Fab/PEG-SiNWFETs as well as their corresponding signal enhancement by R18 aptamer in this study. Voltage shift in presence 0 ng/ml, 0.1 ng/mL, and 1 ng/mL of rabbit IgG, in 150 mM BTP (Bis-Tris propane). From [93]

Other inorganic nanomaterials – based field effect transistors for the affinity sensing (Table 5)

The layers of the 2D material molybdenum disulfide (MoS_2) are held together by weak van der Waals forces and a pristine MoS_2 monolayer presents only ~0.65 nm thick. Monolayer MoS_2 exhibits a direct energy bandgap of ~1.9 eV which lowers leakage current and makes it an emerging material for designing highly sensitive FET biosensors. In all the published works published since 2015, multilayers of MoS_2 were grown or deposited as exfoliated flakes on Si/SiO_2. A Al_2O_3 nanofilm was deposited on the MoS_2 layer, as a dielectric layer, for the protection of the device from the liquid erosion and enhance the electrostatic charge effect of the target molecules. Back-gated FET structures were prepared. Biomarkers for different diseases were detected with these MoS_2-based

FETs: mental stress [95], cardiovascular disease [96], colonic schistosomiasis [97], prostate cancer [98]. Detection limits in the range of fM were obtained.

Nanostructured zinc oxide (ZnO) is a semiconductor with a wide bandgap energy of 3.37 eV. ZnO is a suitable material for biosensing applications due to its biocompatibility with low toxicity to humans and a high isoelectric point. The tuning of the surface defects in an electrolyte-gated ZnO FET biosensor, by the modification of the experimental conditions of electron beam evaporation, allowed to ensure a low detection limit of PSA, the biomarker of prostate cancer, and to assure a reliable long term performance [99].
A bilayer amorphous indium gallium zinc oxide (a-IGZO) was fabricated by changing the partial pressure of O2 in the chamber to fabricate bilayers with different amounts of O vacancies, the low-O vacancy layer on top of the active layer, without extra passivation layers [100]. The electrolyte gated FET, after the immobilization of biotin, through APTES grafting on the a-IGZO surface, allowed the detection of streptavidin with a detection limit 1 pg/mL, with a good selectivity.
A microfluidic field-effect transistor biosensor made of a rolled-up indium nitride microtube was conceived in order to reduce the electrostatic screening of the biosensing surface and then prove the device sensitivity for charge detection in electrolytic environments [101]. The scheme of the microfluidic device is presented in Fig. 11.

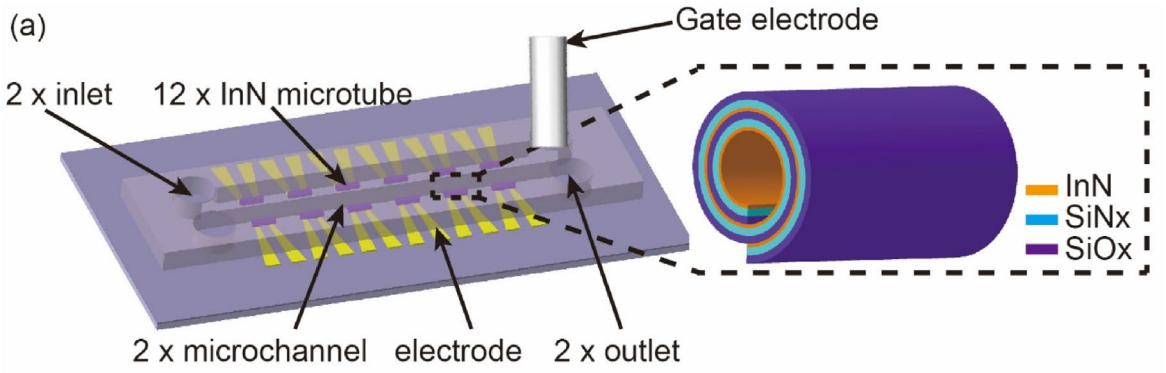

Figure 11. Scheme of the InN microtube based FET biosensor enclosed in a microfluidic channel. From [101].

The detection limit for HIV-1 pg41 antibody, in 0.01xPBS solution is 0.1 ng/mL, which is 20 times lower than that obtained with the standard ELISA kit.
Nanostructured indium oxide (In_2O_3) is a semiconductor with a bandgap energy of 2.8 eV. The affinity of an aptamer for dopamine was determined in artificial cerebrospinal fluid, showing that identified aptamer adopts a conformation optimized for indium oxide based FET detection of dopamine when Mg^{2+} and $Ca2^{+}$ are present. Moreover, this aptamer was found to show high for dopamine versus norepinephrine, as well as other metabolites. The detection limit for dopamine was found to be 10 fM [102].

Carbon nanotube field-effect transistors for affinity sensing (Table 6)

Carbon nanotubes can be obtained with metallic or semi-conducting properties. For the fabrication of CNT-FET, CNTs are deposited from a dispersion of CNTs [104], [105], [106], [108], [110], [111], [112] or CNTs are directly grown on the Si/SiO_2 substrate [103], [106], [109].

Horizontally aligned p-type CNTs are obtained by a controlled chemical vapor deposition (CVD) growth [103] and suspended CNTs between platinum electrodes were fabricated by utilizing the surface tension of liquid silver [109]. The resistance of the CNTs increased leading to a decrease of the drain current of the liquid gated CNT-FET, when the hybridization of DNA increased [109]. The same effect was obtained with the immunodetection of interleukin 6 [103].

When a dispersion of CNTs in dichlorobenzene is deposited on a Kapton surface, a network of CNTs is formed. The network consists predominantly of CNT bundles with some individual CNTs. The small number of metallic (m) tubes and semiconducting tubes of different bandgap (s') than the principal s-CNT lead to the formation of m-s junctions and s-s' junctions in the network in addition to m-m and s-s connections. The detection of potassium ion through a liquid-gated CNT-FET functionalized by a specific aptamer presents a sensitivity of response depending on the time of deposition of the CNT dispersion (Fig. 12A). The sensitivity of detection has been related to the increased dominance of key m-s junctions on the conductance of network's close to percolation, as shown on the scheme presented in Fig. 11B [113].

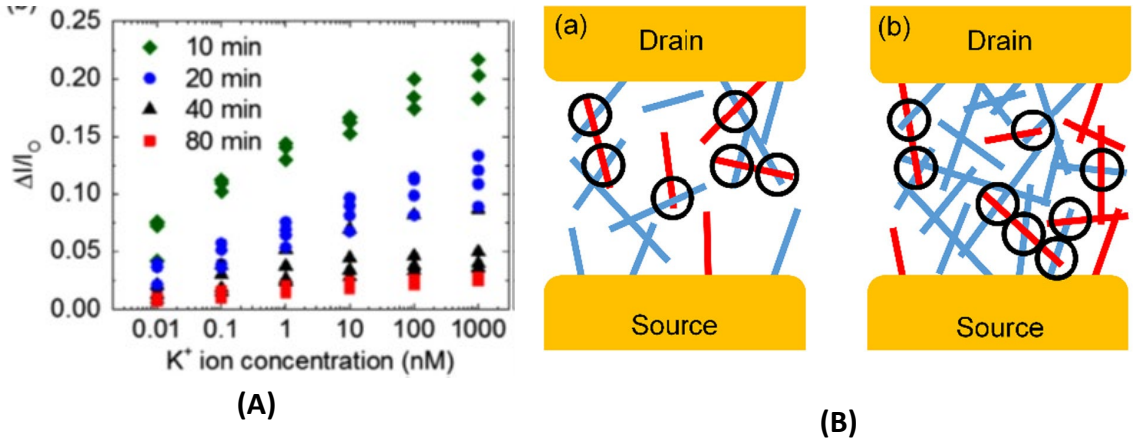

Figure 12. (A) Current response of liquid gated aptasensors normalized with respect to the zero-potassium concentration Io fabricated with CNT networks deposited for 10, 20, 40 and 80 min. (B) Schematic of the formation of metal-semiconducting CNT bundle junctions on a (a) sparse (10 min) and (b) dense CNT network (80 min). Bundles with only semiconducting tubes are in blue and those with metallic tubes are in red. The metal-semiconducting junctions are circled. From [113].

The CNT-FETs for affinity sensing described in the papers published since 2015 allow the detection of biomarkers for different diseases: Acute Respiratory Syndrome [103], cancer [106], oral cancer [107], acute myocardial infarction [110]. Other CNT-FETs allow the

detection of microorganisms: bacteria [111] and of COVID-19 [112]. Hazardous priority substances were detected by CNT-FETs: alkylphenol [104], atrazine [105].

Graphene field-effect transistors for affinity sensing (Table 7)

Due to the extraordinary electrical properties of graphene, since 2015, more than fifty papers report affinity sensors based on graphene field-effect transistors (G-FET). Graphene is made up of carbon atoms which are bound to three others with a 120° bond angle, resulting in a hexagonal lattice arrangement of sp^2-hybrised carbon with a high specific surface area (2630 m^2/g). For the CVD fabrication of graphene films, the carbon atoms decomposed from diverse hydrocarbon sources at high temperatures diffuse on the metal substrate to form initial nuclei, which further expand and coalesce to form graphene layers. The growth procedure will end once the substrates are fully covered with a graphene film, which is mainly referred to as the so-called "self-limiting surface reaction mechanism" that has been observed in Cu and on Ni. After one decade of research efforts, PMMA poly(methyl methacrylate)) is still the most widely used polymer to support the graphene film (one or two layers, with a minimum of cracks) during the transfer process due to its prominent features like transparency, cheapness, easy manipulation, flexibility and solubility in several organic solvents [116,125,126,128,135,136,139,140,3,145,146,150,160]. Small domains of graphene can also be obtained as reduced graphene oxide, graphene oxide being obtained from graphite by the modified Hummers' method [115,117, 131,133,143,144,152,153,154,156,158].
Carrier mobilities in graphene have been reported to be about 2 orders of magnitude larger than in the "gold-standard" semiconductor, silicon. Intrinsic graphene is a gapless semiconductor with a charge neutrality point or Dirac point (where the graphene character changes from being electron-like to hole-like) at the Fermi surface with no free carriers at T = 0 K. This system has an empty conduction band and filled valence band; infinitesimal doping using an external gate voltage (back-gate (Fig. 13A) or liquid-gate (Fig. 13B) in a field-effect transistor, generates the electron transition from the valence to conductance band, thereby changing the intrinsic state to the extrinsic one. By varying the external gate voltage, the system is tuned from being electron-like to being hole-like through its intrinsic nature at the charge neutrality point (CNP), then transducing graphene's ambipolar behavior (Fig. 13C).

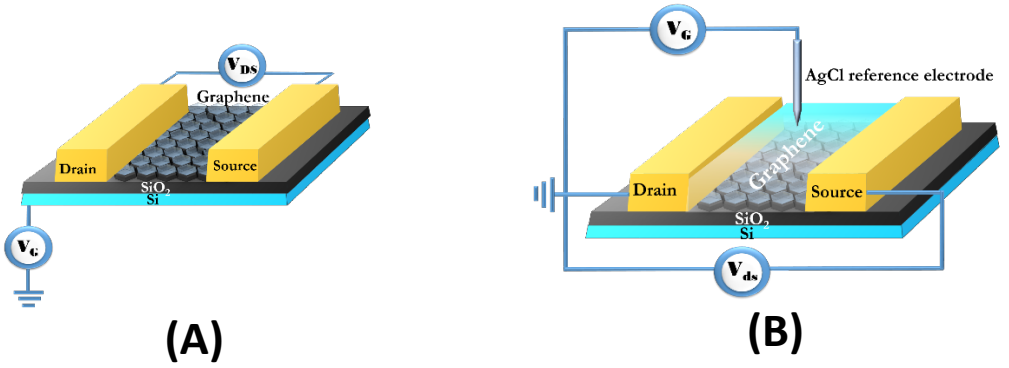

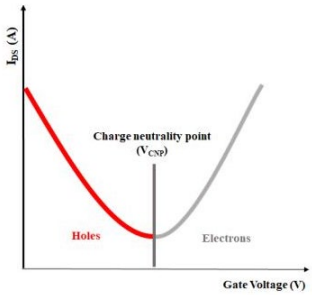

(C)

Figure 13. (A) Back-gated graphene field effect transistor. (B) Liquid-gated graphene field effect transistor. (C) typical ambipolar transfer characteristics of GFET showing that two types of carriers in graphene can continuously be modulated from holes (red color) to electrons (grey color) using the field effect. The V_{CNP} is located at the transition between the hole and electron regime.

A graphene biosensor-based FET works mainly by electrostatic gating effect, which is defined as a consequence of an additional effective gate voltage formed by the collection of the adsorbed biomolecules within the Debye screening length. Such drain current variation can be used as a sensing metric for biomolecule's adsorption. Another type of sensing metric is to follow the transconductance variation through the slope of the transfer curve's linear part of the p or n branch. Additionally, the ambipolar behavior of the GFET devices offers a supplementary sensing mechanism through the measurement of the Dirac point shifting (ΔV_D) or of the charge neutrality point (ΔV_{CNP}) in the function of the surface charge-induced concentration.

For the immobilization of the receptor molecules, covalent functionalization of the graphene surface causes considerable variation in the graphene structure including altering electronic properties caused by the disruption of π electrons and transformation of the carbon atoms hybridization from sp^2- to sp^3-hybridized state. The non-covalent functionalization using the specific aromatic linker molecules like PBASE (1-pyrenebutanoic acid succinimidyl ester) (Fig. 14), which are possibly anchored onto the graphene surface via π- π interaction, does not alter the graphene's electrical properties or its structural integrity.

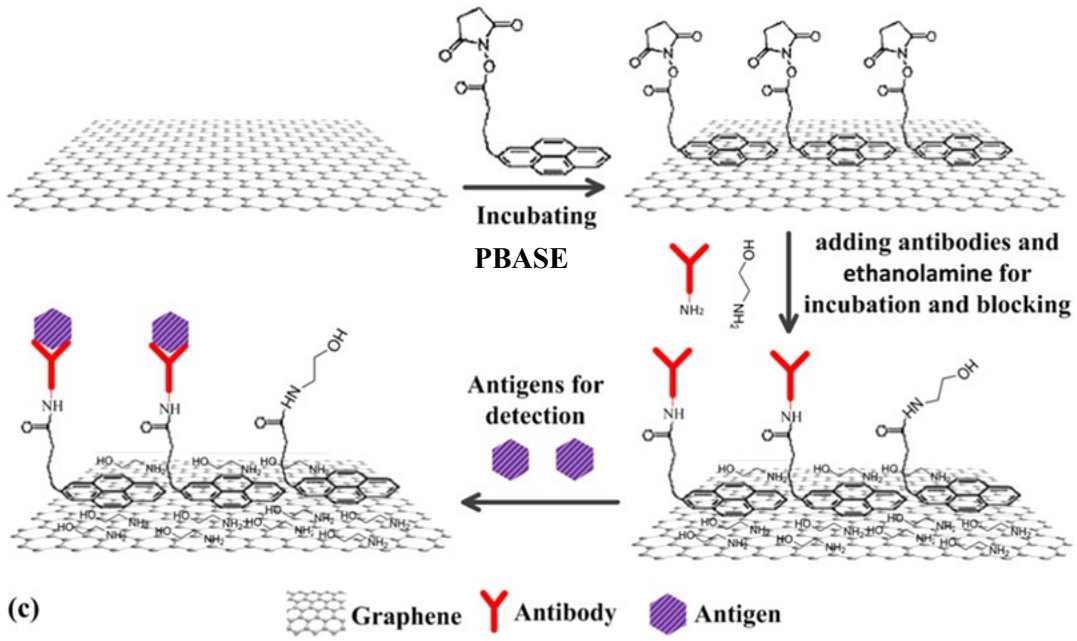

Figure 14. The schematic diagram of the antibody immobilization using the specific aromatic linker molecule PBASE. From [9]

A positive shift of the Dirac point is observed (Fig. 15B), explained by a p-doping effect *via* charge transfer between pyrene unit and graphene. A positive shift of 0.20 V was observed by Seo et al [3], a more positive shift is observed after the immobilization of the SARS-CoV-2 spike antibody. This charge transfer is also corroborated by the conductivity of the graphene layer which is lower in presence of PBASE (Fig. 15A).

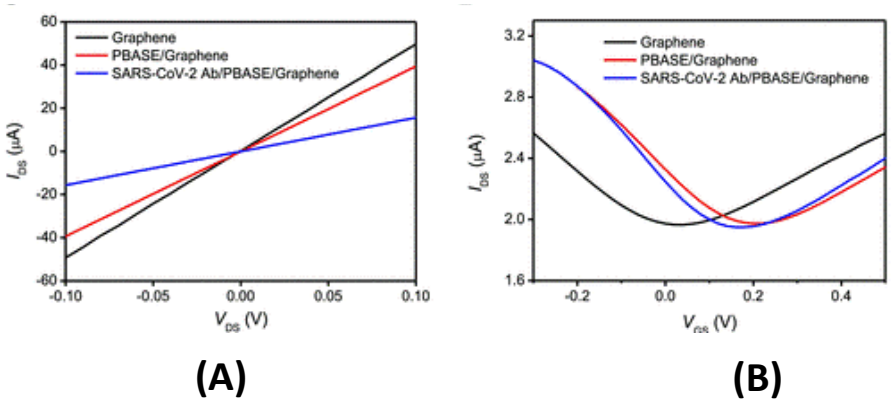

Figure 15. Electrical characterization of pristine, PBASE-modified and SARS-CoV-2 spike antibody-immobilized graphene. (A) Current-voltage (I-V) characteristics of the graphene-based device at each functionalization process for the antibody immobilization. (D) Measurement of transfer curve of the COVID-19 FET sensor in steps of the antibody conjugation (V_{DS} = 0.01V). [from 3]

In addition to diluting the buffer salt concentration, the use of polymers such as polyethylene glycol (PEG) co-immobilization could locally reduce the Debye screening effect near the vicinity of the biorecognition molecules. Following this strategy, Andoy et al [135] used graphene modified with aptamer and PEG for thyroid-stimulating hormone (TSH) detection. The developed GFETs exhibited a very low LOD ($\simeq$0.2x 10^{-15} M) and a high sensitivity toward THS protein in high ionic strength and whole serum.

Nonetheless, designing short receptors is still the preferable approach for several research groups. It is an effective and straightforward method to reduce the distance separating the transistor surface and biomolecule analytes. This point was demonstrated by Kanai et al [142] who used an antibody variable fragment for the detection of a small antigen peptide through an open-sandwich immunoassay based on a liquid-gated G-FET. The sensitivity was increased by a factor 10, compared to an ELSA test.

Whereas the extremely low LOD of 600 zM in buffer solution was recorded by Hwang et al [146] who developed a deformed (crumpled) graphene monolayer channel (Fig. 16) for miRNA detection based on FET biosensors. The critical factor in reaching such lower LOD values depends on the following strategy to overcome the Debye length screening effect. Hwang et al. combined the benefits of the uncharged and short structure of PNA with the advantage of crumpled graphene surface which allows a larger shift of the Dirac point, compared to flat graphene surface (Fig. 17).

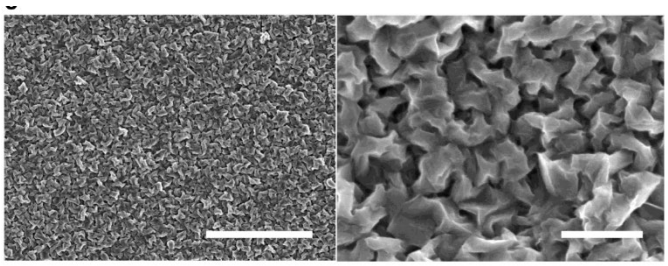

Figure 16. SEM image of crumpled graphene. The scale bar is 5 µm (left) and 500 nm (right). From [146]

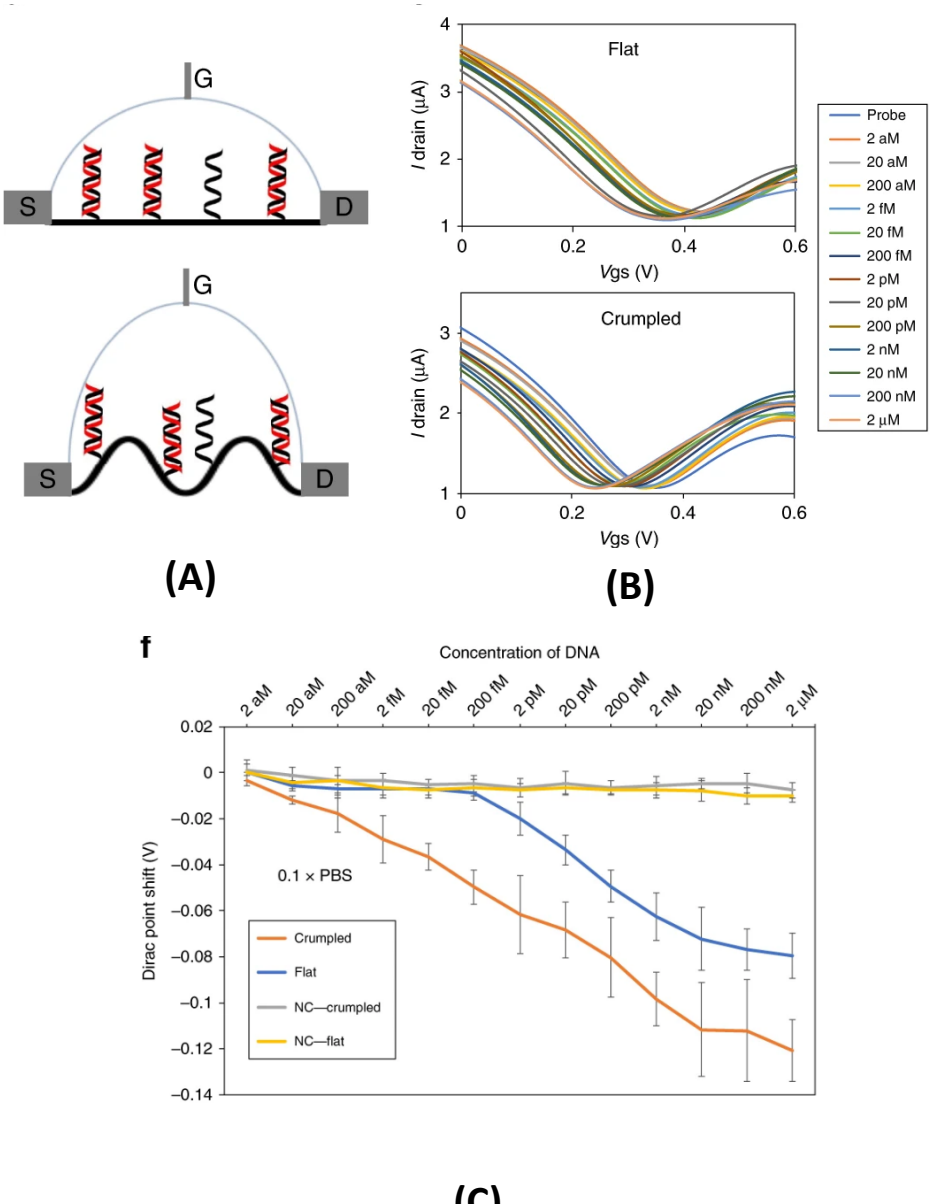

Figure 17. (A) Lateral image of the flat (top) and crumpled (bottom) graphene FETDNA sensors. DNA (red strand) is hybridized with probe DNA (black strand) on the graphene surface. (B) I-V relationship of the flat (top) and crumpled (bottom) graphene FET sensors for the DNA hybridization. DNA hybridization shifted the I-V curve according to the indicated concentrations. The I-V curves shift of crumpled graphene is significantly larger than the flat device. (C) Dirac voltage shift of the FET sensor with detection of hybridization using DNA probe. NC is non-complementary control sequences used in the experiments. From [146].

The numerous graphene FET developed since 2015 allow the detection of biomarkers of different diseases: tuberculosis [118,162], cancer [122,133,134,140,144,153,160], trophoblastic tumors [125,126,132], mental stress [129,151,164], hyperthyroidism [135], cardiovascular disorder [139], rheumatoid arthritis [139], HIV [139], bone disease [142], Alzheimer's disease [147,161], heart failure [158]. Some of them allow the detection of

virus: Hepatitis B [119,131], COVID-19 [3,149,154], japanese encephalitis [148], avian influenza [148], human papillomavirus [156], the detection of toxins: aflatoxin B1 117], okadaic acid [130], geosmin [155], the detection of drugs [157] and the detection of a pesticide, chlorpyrifos [138]. Many G-FET were used for the detection of DNA sequences [114,116,120,121,123,124,137,141,146,150,152,159,163], of miRNA [115], RNA [128].
When comparing the analytical performance of G-FET for the detection of cortisol, it is observed that an electrolyte-gated G-FET, based on graphene nanoplatelets functionalized with a monoclonal cortisol antibody [129] gave a detection limit of 10 pg/mL and a dynamic range of 10 pg/mL – 10 µg/mL, another electrolyte-gated G-FET, based on graphene nanoplatelets functionalized with a mouse monoclonal cortisol antibody [151] gave a detection limit of 0.85 ng/mL and a dynamic range of 1 pg/mL – 10 ng/mL and a last extended gate G-FET, based on a platinum extended gate electrode coved with a single-layer graphene decorated with a 61-basepair aptamer [164] gave a detection limit of 0.2 nM (72.4 ng/mL) and a dynamic range of 1 nM (362 pg/mL) – 10 µM (3.62 µg/mL). In the third G-FET, the use of a short aptamer allows the detection in the Debye layer; nevertheless the same amplitude (3 decades) of dynamic range was also obtained with the antibody functionalized G-FET [130] which can be explained by the Donnan effect [2].
About the detection of hepatitis B virus, three G-FETs were functionalized with a monoclonal antibody, two of them were based on graphene nanogrids (graphene deposited on nanoporous silicon oxide through electrophoretic deposition method) and led to a limit of detection of 0.05 fM [119] and 0.1 fM [131] Hep-B virus , the other one is based on deposition of ERGO on FTO covered glass and led to a detection limit of 1 fM [143], due to a lower quality of graphene.

Comparison of the detection limits obtained with the different types of FET based affinity sensors

Cortisol, a biomarker of mental stress was detected with different types of FETs: with silicon based FET a detection limit of 50 µM was obtained [52]; with AlGaN/GaN FET, a detection limit of 1 pM was obtained [68]; with OFET detection limits of 2.76 pM [75] and 27.3 pM [76] were obtained; with MoS_2 based FET, a detection limit of 2.76 aM was obtained [95]; with graphene based FET, detection limits of 27.6 pM [129], 2.34 pM [151] and 0.2 nM [164] were obtained. From this comparison, it comes that silicon based FET gives a detection limit in the range of micromolar while the other FET gave a detection limit in the range of picomolar. A very low detection limit was obtained with a MoS_2 based FET, in the range of attomolar.

Prostate specific antigen (PSA) is a biomarker of prostate cancer, its molecular weight is 30000 Daltons. It was detected with different types of FETs: with AlGaN/GaN FET detection limits of 100 fg/mL [65] and of 1 ng/mL [67] were obtained; with Si NW FET, a detection limit of 23 fg/mL [86]; with MoS_2 based FET, a detection limit of 1fg/mL was obtained [98]; with ZnO FET, a detection limit of 0.06 fM (2.4 ag/mL) was obtained [99]; with graphene FET, a detection limit of 1 pg/mL was obtained [153]. From this comparison, it appears that

the lower detection limits are obtained with the nanomaterials based FET, in the range of femtogram per milliliter, the lower one being obtained with ZnO FET.

The detection of DNA was performed with different types of FET: with silicon based FET, a detection limit of 1 µM was obtained [56]; with AlGaN/GaN FET a detection limit of 10 fM was obtained [62]; with OFET a detection limit of 9.77 pM was obtained [81]; with SWCNT FET a detection limit of 10 aM was obtained [109]; with graphene FET, ten DNA sensors were reported with different detection limits from 10 nM [124,159], 1 nM [152], 1 pM [123], 100 fM [114], 2.3 fM [141], 1 fM [116,121], 10 aM [150], 600 zM [146]. From this comparison, it appears that the lower detection limits are obtained with SWCNT FETs and with graphene FETs. Both carbonaceous nanomaterials based FETs present the higher field effect for the detection of DNA hybridization compared to the other nanomaterials. The lower detection limit was reached with crumpled graphene [146], this morphology modifying the Debye length which increases in the concave regions [165].

Summary and Perspectives.

This review shows that nanomaterials based field effect transistors for the affinity sensing of biomarkers and of DNA sequences present a growing interest for the scientific community. Very low detection limits and very short response time, compared to classical ELISA tests were obtained.

From the number of the recently published works on the affinity sensors based on field-effect transistors, the graphene-FETs appear to be the more popular. Due to the production of CVD-grown graphene on CU catalyst with large scale, the window towards industrial-scale production of high quality graphene is opened. To accelerate commercialization of high-efficient G-FET, the transfer technique should be optimized in terms of graphene quality and of environment friendly process.

Acknowledgements

The authors acknowledge the financial support of the EU H2020 WIDESPREAD Program entitled Bionanosens grant agreement # 951887.

References

[1] P. Bergveld, Thirty years of ISFETOLOGY What happened in the past 30 years and what may happen in the next 30 years. Sensors and Actuators B 88 (2003) 1–20. https://doi.org/10.1016/S0925-4005(02)00301-5

[2] M. Kaisti. Detection principles of biological and chemical FET sensors. Biosensors & Biolectronics 2017, 98, 437-448. https://doi.org/10.1016/j.bios.2017.07.010

[3] G. Seo, G. Lee, M. J Kim, S.H. Baek, M. Choi, K.B. Ku, Ch-S. Lee, S. Jun, D. Park, H.G. Kim, S.J. Kim, J.O. Lee, B.T. Kim, E. Ch Park, S. Il Kim, Rapid detection of COVID-19 causative virus (SARS-CoV-2) in human nasopharyngeal swab specimens using field-effect transistor- based biosensor, *ACS Nano* **2020**, *14*, 5135–5142. https://doi.org/10.1021/acsnano.0c02823.

[4] D. Barcelo, Wastewater-based epidemiology to monitor COVID-19 outbreak: present and future diagnostic methods to be in your radar. *Case Stud. Chem. Environ. Eng.* **2020**, *2*, 100042. https://doi.org/10.1016/j.cscee.2020.100042

[5] R. Antiochia, Nanobiosensors as new diagnostic tools for SARS, MERS and COVID-19: from past to perspectives. *Microchim. Acta* **2020**, *187*, 639. https://doi.org/10.1007/s00604-020-04615-x

[6] K.S.V. Santharam, Electrochemical approaches towards sensing viruses: A mini review. *Med. Devices Sens.* **2021**, *4*, e10148. https://doi.org/10.1002/mds3.10148

[7] A. Poghossian, M. Jablonski, D. Molinnus, C. Wege, M.J. Schöning. Field-effect sensors for virus detection: from Ebola to SARS-CoV-2 and plant viral enhancers. *Front. Plant Sci.* **2020**, *11*, 598103. https://doi.org/10.3389/fpls.2020.598103

[8] A.D. Teklemariam, M. Samaddar, M.G. Alharbi, R.R. Al-Hindi, A.K. Bhunia. Biosensors and molecular-based methods for the detection of human coronaviruses: a review. *Mol. Cell. Probes* **2020**, *54*, 101662. https://doi.org/10.1016/j.mcp.2020.101662

[9] S. Forouhi, E. Ghafar-Zadeh. Applications of CMOS devices for the diagnosis and control of infectious diseases. *Micromachines* **2020**, *11*, 1003. http://doi.org/10.3390/mi11111003

[10] M. Srivastava, N. Srivastava, P.K. Mishra, B.D. Malhotra. Prospects of nanomaterials-enabled biosensors for COVID-19 detection. *Sci. Total Environ.* **2021**, *754*, 142363. https://doi.org/10.1016/j.scitotenv2020.142363

[11] S. Suleman, S.K. Shukla, N. Malhotra, S.D. Bukkitgar, N.P. Shetti, R. Pilloton, J. Narang, Y.N. Tan, T.M. Aminabhavi. Point of care detection of COVID-19: Advancement in biosensing and diagnostic methods. *Chem. Eng. J.* **2021**, *414*, 128759. https://doi.org/10.1016/j.cej.2021.128759

[12] N.P. Shetti, A. Mishra, S.D. Bukkitgar, S. Basu, J. Narang, K.R. Reddy, T.M. Aminabhavi. Conventional and nanotechnology-based sensing methods for SARS coronavirus (2019-nCOV). *ACS Appl. Bio Mater.* 2021, 4, 1178-1190. https://doi.org/10.1021/acsabm.0c01545

[13] K.Y. Goud, K.K. Reddy, A. Khorshed, V.S. Kumar, R.K. Mishra, M. Oraby, A.H. Ibrahim, H. Kim, K.V. Gobi. Electrochemical diagnostics of infectious viral diseases: Trends and challenges. *Biosens. Bioelectron.* **2021**, *180*, 113112. https://doi.org/10.1016/j.bios.2021.113112

[14] A. Panahi, D. Sadighbayan, S. Forouhi, E. Ghafar-Zadeh. Recentadvances of field-effect transistor technologye for infectious diseases. Biosensors 2021, 11, 103. http://doi.org/10.3390/bios11040103

[15] A. Rhouati, A. Teniou, M. Badea, J.L. Marty. Analysis of recent bio-/nanotechnologies for coronavirus diagnosis and therapy. Sensors 2021, 21, 1485. https://doi.org/10.3390/s21041485

[16] X. Chen, T. Dong, X. Wei, Z. Yang, N.M.M. Pires, J. Ren, Z. Jiang. Electrochemical methods for detection of biomarkers of chronic obstructive pulmonary disease in serum and saliva. *Biosens. Bioelectron.* **2019**, *142*, 111453. https://doi.org/10.1016/j.bios.2019.111453

[17] P. Salvo, F.M. Vivaldi, A. Bonini, D. Biagini, F.G. Bellagambi, F.M. Miliani, F. Di Francesco, T. Lomonaco. Biosensors for detecting lymphocytes and immunoglobulins. *Biosensors* **2020**, *10*, 155. https://doi.org/10.3390/bios10110155

[18] B. Li, H. Tan, D. Jenkins, V.S. Raghavan, B.G. Rosa, F. Güder, G. Pan, E. Yeatman, D.J. Sharp. Clinical detection of neurodegenerative blood biomarkers using graphene immunosensor. *Carbon* **2020**, *168*, 144-162. https://doi.org/10.1016/j.carbon.2020.06.048

[19] P. Sharma, A. Panchal, N. Yadav, J. Narang, Analytical techniques for the detection of glycated haemoglobin underlining sensors. *Intern. J. Biol. Macromol.* **2010**, *155*, 685-696. https://doi.org/10.1016/j.ijbiomac.2020.03.205

[20] P. Mohankumar, J. Ajayan, T. Mohanraj, R. Yasodharan, Recent developments in biosensors for healthcare and biomedical applications: a review. *Measurements* **2021**, *167*, 108293. https://doi.org/10.1016/j.measurement.2020.108293

[21] S. Dolati, J. Soleymani, S.K. Shakouri, A. Mobed. The trends in nanomaterial-based biosensors for detecting critical biomarkers in stroke. Clinica Chimica Acta, 2021, 514, 107-121. http://doi.org/10.1016/j.cca.2020.12.034

[22] F. Farshchi, M. Hasanzadeh, Microfluidic biosensing of circulating tumor cells (CTCs): Recent progress and challenges in efficient diagnosis of cancer. *Biomed. Pharmacother.* **2021**, *134*, 111153. http://doi.org/10.1016/j.biopharma.2020.111153

[23] K. Malecka, E. Mikula, E.E. Ferapontova. Design strategies for electrochemical aptasensors for cancer diagnostic devices. *Sensors* **2021**, *21*, 736. https://doi.org/10.3390/s21030736

[24] C. Ibau, M.K.M. Arshad, S.C.B. Gopinath. Current advances and future visions on bioelectronic immunosensing for prostate-specific antigen. Biosensors and Bioelectronics 2017, 98, 267-284. http://doi.org/10.1016/j.bios.2017.06.049

[25] D. Sadighbayan, M. Hasanzadeh, E. Ghafar-Zadeh. Biosensing based on field-effect transistors (FET): Recent progress and challenges. Trends in Analytical Chemistry 2020, 133, 116067. http://doi.org/10.1016/j.trac.2020.116067

[26] V. Kumar, K. Vaid, S.A. Bansal, K.H. Kim. Nanomaterial-based immunosensors for ultrasensitive detection of pesticides/herbicides: Current status and perspectives. *Biosens. Bioelectron.* **2020**, *165*, 112382. https://doi.org/10.1016/j.bios.2020.112382

[27] I. Ben Chabchoubi, N. Belkhamssa, M. Ksibi, O. Hentati, Trends in the detection of pharmaceuticals and endocrine-disrupting compounds by Field-Effect Transistors (FETS). *Trends Environ. Anal. Chem.* 2021, 30, e00127. https://doi.org/10.1016/j.teac.2021.e00127

[28] S. Szunerits, R. Boukherroub, Graphene-based bioelectrochemistry and bioelectronics : A concept for the future? Current Opinion in Electrochemistry **2018**, *12*, 141-147. https://doi.org/10.1016/j.coelec.2018.03.028

[29] I. Prattis, E. Hui, P. Gubeljak, G.S. Kaminski Schierle, A. Lombardo, L.G. Occhipinti. Graphene for biosensing applications in point-of-care testing. Trends in Biochemistry **2021**. https://doi.org/10.1016/j.tibtech.2021.01.005

[30] M. Singh, N. Kaur, E. Comini, The role of self-assembled monolayers in electronic devices. Journal of Materials Chemistry C **2020**, *8*, 3938-3955. https://doi.org/10.1039/d0tc00388c

[31] S. Kim, H. Yoo. Self-assembled monolayers: versatile uses in electronic devices from gate dielectrics, dopants and biosensing linkers. Micromachines **2021**, *12*, 565. https://doi.org/10.3390/mi12050565

[32] K.T. Upadhyay, M.K. Chattopadhyay. Sensor application based on AlGaN/GaN heterostructures. Materials Science & Engineering B **2021**, *263*, 114849. https://doi.org/10.116/j.mseb.2020.114849

[33] A. Zhang, J.H. Lee, C.M. Lieber. Nanowire-enabled bioelectronics. Nano Today 2021, 38, 101135. https://doi.org/10.1016/j.nanotd.2021.101135

[34] S. Hannah, E. Blair, D.K. Corrigan. Developments in microscale and nanoscale sensors for biomedical sensing. Current Opinion in Electrochemistry 2020, 23, 7-15. https://doi.org/10.1016/j.coelec.2020.02.012.

[35] T. Sakata, S. Nishitani, T. Kajisa.Molecularly imprinted polymer-based bioelectrical interfaces with intrinsic molecular charges. RSC Advances 2020, 10, 16999. https://doi.org/10.1039/d0ra02793f

[36] I.M. Bhattacharyya, S. Cohen, A. Shalabny, M. Bashouti, B. Akabayov, G. Shalev. Specific and label-free immunsensing of protein-protein interactions with silicon-based immunoFETs. Biosensors & Bioelectronics 2019, 132, 143-161. https://di.org/10.1016/j.bios.2019.03.003

[37] C. Kotlowski, P. Aspermair, H. Ullah Khan, C. Reiner-Rozman, J. Breu, S. Szunerits, J.J. Kim, Z. Bao, C. Kleber, P. Pelosi, W. Knoll. Electronic biosensing with flexible organic transistor devices. Flexible Printed Electronics 2018, 3, 034003. https://doi.org/10.1088/2058-8585/aad433

[38] T. Minamiki, Y. Sasaki, S. Su, T. Minami. Developement of polymer field-effect transistor-based immunosensors. Polymer Journal 2019, 51, 1-9. https://doi.org/10.1038/s41428-018-0112-0

[39] M.L. Coluccio, S.A. Pullano, M.F.M. Vismara, N. Coppede, G. Perozziello, P. Candeloro, F. Gentile, N. Malara. Emerging designs of electronic devices in biomedicine. Micromachines 2020, 11, 123. https://doi.org/10.3390/mi11020123

[40] R.A. Picca, K. Manoli, E. Macchia, L. Sarcina, C. Di Franco, N. Cioffi, D. Blasi, R. Osterbacka, F. Torricelli, G. Scamarcio, L. Torsi. Ultimately sensitive organic biolectronic transistor sensors by materials and device structure design. Advanced Functional Materials 2020, 30, 1904513. https://doi.org/10.1002/adfm.201904513

[41] X. Yao, Y. Zhang, W. Jin, Y. Hu, Y. Cui. Carbon nanotube field-effect transistor-based chemical and biological sensors. Sensors 2021, 21, 995. https://doi.org/10.3390/s21030995

[42] R. Forsyth, A. Devadoss, O.J. Guy. Graphene field effect transistors for biomedical applications: Curent status and future prospects. Diagnostics 2017, 7, 45. https://doi.org/10.3390/diagnostics7030045

[43] S. Mao. Graphene field-effect transistor sensors in “Graphene Bioelectronics”, Ed. A. Tiwari, Elsevier 2017. **eBook ISBN:** 9780128133507

[44] K. Laxmi, B. Mahapatra, R.V. Krishna, P.K. Patel. A review of recent advancements in graphene based field-effect transistor biosensors. AIP Conference Proceeding 2021, 2327, 020011. https://doi.org/10.1063/5.0039650

[45] R. Ahmad, T. Mahmoudi, M.S. Ahn, Y.B. Hahn. Recent advances in nanowires-based field-effect transistors for biological sensor applications. Biosensors & Bioelectronics 2018, 100, 312-325. https://doi.org/10.1016/j.bios.2017.09.024.

[46] A.C. Mazarin de Moraes, L.T. Kubota. Recent trends in field-effect transistors-based immunosensors. Chemosensors 2016, 4, 20. https://doi.org/10.3390/chemosensors4040020

[47] C.A. Vu, W.Y. Chen. Field-effect transistor biosensors for biomedical applications: recent advances and future prospects. Sensors 2019, 19, 4214. https://doi.org/1.3390/s19194214

[48] D. Sung, J. Koo. A review of BioFET’s basic principles and materials for biomedical applications. Biomedical Engineering Letters 2021, 11, 85-96. https://doi.org/10.1007/s13534-021-00187-8

[49] S. Cheng, S. Hideshima, S. Kuroiwa, T. Nakanishi, T. Osaka, Label-free detection of tumor markers using field effect transistor (FET)-based biosensors for lung cancer diagnosis, Sensors and Actuators B: Chemical. 212 (2015) 329–334. https://doi.org/10.1016/j.snb.2015.02.038.

[50] H.-J. Jang, J. Ahn, M.-G. Kim, Y.-B. Shin, M. Jeun, W.-J. Cho, K.H. Lee, Electrical signaling of enzyme-linked immunosorbent assays with an ion-sensitive field-effect transistor, Biosensors and Bioelectronics. 64 (2015) 318–323. https://doi.org/10.1016/j.bios.2014.09.020.

[51] S. Hideshima, H. Hayashi, H. Hinou, S. Nambuya, S. Kuroiwa, T. Nakanishi, T. Momma, S.-I. Nishimura, Y. Sakoda, T. Osaka, Glycan-immobilized dual-channel field effect transistor biosensor for the rapid identification of pandemic influenza viral particles, Sci Rep. 9 (2019) 11616. https://doi.org/10.1038/s41598-019-48076-6.

[52] H. Hayashi, R. Toyama, R. Takibuchi, S. Hideshima, S. Kuroiwa, N. Kaneko, K. Horii, K. Ohashi, T. Momma, T. Osaka, Immobilization of Target-Bound Aptamer on Field Effect Transistor Biosensor to Improve Sensitivity for Detection of Uncharged Cortisol, Electrochemistry. advpub (2020). https://doi.org/10.5796/electrochemistry.20-00144.

[53] K.K. Han, S. Mangmool, K. Sathirakul, K. Chansiri, W. Jeamsaksiri, M. Yasawong, Development of immunoFET biosensor for detection of 3-nitrotyrosine, Thai Journal of Pharmaceutical Sciences (TJPS). 44 (2020).

[54] D. Vozgirdaite, H. Ben Halima, F.G. Bellagambi, A. Alcacer, F. Palacio, N. Jaffrezic-Renault, N. Zine, J. Bausells, A. Elaissari, A. Errachid, Development of an ImmunoFET for Analysis of Tumour Necrosis Factor-α in Artificial Saliva: Application for Heart Failure Monitoring, Chemosensors. 9 (2021) 26. https://doi.org/10.3390/chemosensors9020026.

[55] H. Ben Halima, F.G. Bellagambi, A. Alcacer, N. Pfeiffer, A. Heuberger, M. Hangouët, N. Zine, J. Bausells, A. Elaissari, A. Errachid, A silicon nitride ISFET based immunosensor for tumor necrosis factor-alpha detection in saliva. A promising tool for heart failure monitoring, Analytica Chimica Acta. 1161 (2021) 338468. https://doi.org/10.1016/j.aca.2021.338468.

[56] M. Kaisti, A. Kerko, E. Aarikka, P. Saviranta, Z. Boeva, T. Soukka, A. Lehmusvuori, Real-time wash-free detection of unlabeled PNA-DNA hybridization using discrete FET sensor, Sci Rep. 7 (2017) 15734. https://doi.org/10.1038/s41598-017-16028-7.

[57] Ó. Gutiérrez-Sanz, N. Haustein, M. Schroeter, T. Oelschlaegel, M.S. Filipiak, A. Tarasov, Transistor-based immunosensing in human serum samples without on-site calibration, Sensors and Actuators B: Chemical. 295 (2019) 153–158. https://doi.org/10.1016/j.snb.2019.05.043.

[58] C. Baldacchini, A.F. Montanarella, L. Francioso, M.A. Signore, S. Cannistraro, A.R. Bizzarri, A Reliable BioFET Immunosensor for Detection of p53 Tumour Suppressor in Physiological-Like Environment, Sensors. 20 (2020) 6364. https://doi.org/10.3390/s20216364.

[59] M.-Á. García-Chamé, Ó. Gutiérrez-Sanz, E. Ercan-Herbst, N. Haustein, M.S. Filipiak, D.E. Ehrnhöfer, A. Tarasov, A transistor-based label-free immunosensor for rapid detection of tau protein, Biosensors and Bioelectronics. 159 (2020) 112129. https://doi.org/10.1016/j.bios.2020.112129.

[60] C.-R. Wu, S.-L. Wang, P.-H. Chen, Y.-L. Wang, Y.-R. Wang, J.-C. Chen, Demonstration of the enhancement of gate bias and ionic strength in electric-double-layer field-effect-transistor biosensors, Sensors and Actuators B: Chemical. 334 (2021) 129567. https://doi.org/10.1016/j.snb.2021.129567.

[61] H.H. Lee, M. Bae, S.-H. Jo, J.-K. Shin, D.H. Son, C.-H. Won, H.-M. Jeong, J.-H. Lee, S.-W. Kang, AlGaN/GaN High Electron Mobility Transistor-Based Biosensor for the Detection of C-Reactive Protein, Sensors. 15 (2015) 18416–18426. https://doi.org/10.3390/s150818416.

[62] N. Espinosa, S.U. Schwarz, V. Cimalla, O. Ambacher, Detection of different target-DNA concentrations with highly sensitive AlGaN/GaN high electron mobility transistors, Sensors and Actuators B: Chemical. 210 (2015) 633–639. https://doi.org/10.1016/j.snb.2015.01.019.

[63] C.-H. Chu, I. Sarangadharan, A. Regmi, Y.-W. Chen, C.-P. Hsu, W.-H. Chang, G.-Y. Lee, J.-I. Chyi, C.-C. Chen, S.-C. Shiesh, G.-B. Lee, Y.-L. Wang, Beyond the Debye length in high ionic strength solution: direct protein detection with field-effect transistors (FETs) in human serum, Sci Rep. 7 (2017) 5256. https://doi.org/10.1038/s41598-017-05426-6.

[64] J. Yang, P. Carey, F. Ren, M.A. Mastro, K. Beers, S.J. Pearton, I.I. Kravchenko, Zika virus detection using antibody-immobilized disposable cover glass and AlGaN/GaN high electron mobility transistors, Appl. Phys. Lett. 113 (2018) 032101. https://doi.org/10.1063/1.5029902.

[65] S. Yang, L. Gu, X. Ding, B. Miao, Z. Gu, L. Yang, J. Li, D. Wu, Disposable Gate AlGaN/GaN High-Electron- Mobility Sensor for Trace-Level Biological Detection, IEEE Electron Device Letters. 39 (2018) 1592–1595. https://doi.org/10.1109/LED.2018.2868433.

[66] T.-Y. Tai, A. Sinha, I. Sarangadharan, A.K. Pulikkathodi, S.-L. Wang, G.-Y. Lee, J.-I. Chyi, S.-C. Shiesh, G.-B. Lee, Y.-L. Wang, Design and Demonstration of Tunable Amplified Sensitivity of AlGaN/GaN High Electron Mobility Transistor (HEMT)-Based Biosensors in Human Serum, Anal. Chem. 91 (2019) 5953–5960. https://doi.org/10.1021/acs.analchem.9b00353.

[67] A. Varghese, C. Periasamy, L. Bhargava, Fabrication and Charge Deduction Based Sensitivity Analysis of GaN MOS-HEMT Device for Glucose, MIG, C-erbB-2, KIM-1, and PSA Detection, IEEE Transactions on Nanotechnology. 18 (2019) 747–755. https://doi.org/10.1109/TNANO.2019.2928308.

[68] K. Woo, W. Kang, K. Lee, P. Lee, Y. Kim, T.-S. Yoon, C.-Y. Cho, K.-H. Park, M.-W. Ha, H.H. Lee, Enhancement of cortisol measurement sensitivity by laser illumination for AlGaN/GaN transistor biosensor, Biosensors and Bioelectronics. 159 (2020) 112186. https://doi.org/10.1016/j.bios.2020.112186.

[69] J. Wang, Z. Gu, X. Liu, L. Zhao, H. Peng, J. Li, An electronic enzyme-linked immunosorbent assay platform for protein analysis based on magnetic beads and AlGaN/GaN high electron mobility transistors, Analyst. 145 (2020) 2725–2730. https://doi.org/10.1039/C9AN01809C.

[70] G. Palazzo, D. De Tullio, M. Magliulo, A. mAllardi, F. Intranuovo, M.Y. Mulla, P. Favia, I. Vikholm-Lundin, L. Torsi, Detection beyond Debye's length with an electrolyte-gates organic field-effect transistor, Adv. Mater. 27 (2015) 911-916. https://doi.org/10.1002/adma.201403541.

[71] T. Minamiki, T. Minami, Y. Sasaki, S. Wakida, R. Kurita, O. Niwa, S. Tokito, Label-Free Detection of Human Glycoprotein (CgA) Using an Extended-Gated Organic Transistor-Based Immunosensor, Sensors. 16 (2016) 2033. https://doi.org/10.3390/s16122033.

[72] M. Magliulo, D. De Tullio, I. Vikholm-Lundin, W.M. Albers, T. Munter, K. Manoli, G. Palazzo, L. Torsi, Label-free C-reactive protein electronic detection with an electrolyte-gated organic field-effect transistor-based immunosensor, Anal Bioanal Chem. 408 (2016) 3943–3952. https://doi.org/10.1007/s00216-016-9502-3.

[73] P. Seshadri, K. Manoli, N. Schneiderhan-Marra, U. Anthes, P. Wierzchowiec, K. Bonrad, C. Di Franco, L. Torsi, Low-picomolar, label-free procalcitonin analytical detection with an electrolyte-gated organic field-effect transistor based electronic immunosensor, Biosensors and Bioelectronics. 104 (2018) 113–119. https://doi.org/10.1016/j.bios.2017.12.041.

[74] J. Song, J. Dailey, H. Li, H.J. Jang, P. Zhang, J.T.H. Wang, A.D. Everett, H.E. Katz, Extended solution gate OFET-based biosensor for label-free glial fibrillary acidic protein detection with polyethylene glycol-containing bioreceptor, Adv. Funct. Mater. 27 (2017) 1606506. https://doi.org/10.1002/adfm.201606506

[75] H.-J. Jang, T. Lee, J. Song, L. Russell, H. Li, J. Dailey, P.C. Searson, H.E. Katz, Electronic Cortisol Detection Using an Antibody-Embedded Polymer Coupled to a Field-Effect Transistor, ACS Appl. Mater. Interfaces. 10 (2018) 16233–16237. https://doi.org/10.1021/acsami.7b18855.

[76] R. Massey, S. Bebe, R. Prakash, Aptamer-Enhanced Organic Electrolyte-Gated FET Biosensor for High-Specificity Detection of Cortisol, IEEE Sensors Letters. 4 (2020) 1–4. https://doi.org/10.1109/LSENS.2020.3002446.

[77] M. Sensi, M. Berto, S. Gentile, M. Pinti, A. Conti, G. Pellacani, C. Salvarani, A. Cossarizza, C. Augusto Bortolotti, F. Biscarini, Anti-drug antibody detection with label-free electrolyte-gated organic field-effect transistors, Chemical Communications. 57 (2021) 367–370. https://doi.org/10.1039/D0CC03399E.

[78] J.L. Gall, S. Vasilijević, N. Battaglini, G. Mattana, V. Noël, R. Brayner, B. Piro, Algae-functionalized hydrogel-gated organic field-effect transistor. Application to the detection of herbicides, Electrochimica Acta. 372 (2021) 137881. https://doi.org/10.1016/j.electacta.2021.137881.

[79] C. Sun, R. Li, Y. Song, X. Jiang, C. Zhang, S. Cheng, W. Hu, Ultrasensitive and Reliable Organic Field-Effect Transistor-Based Biosensors in Early Liver Cancer Diagnosis, Anal. Chem. 93 (2021) 6188–6194. https://doi.org/10.1021/acs.analchem.1c00372.

[80] T. Minamiki, T. Minami, Y.-P. Chen, T. Mano, Y. Takeda, K. Fukuda, S. Tokito, Flexible organic thin-film transistor immunosensor printed on a one-micron-thick film, Commun Mater. 2 (2021) 1–8. https://doi.org/10.1038/s43246-020-00112-z.

[81] H.J.N.P.D. Mello, B. Bachour Junior, M. Mulato, Polyaniline-based field effect transistor for DNA/RNA biomarker sensing: Comparison to electrochemical impedance and inorganic layer, Sensors and Actuators A: Physical. 318 (2021) 112481. https://doi.org/10.1016/j.sna.2020.112481.

[82] T. Minamiki, T. Minami, R. Kurita, O. Niwa, S. Wakida, K. Fukuda, S. Tokito, Accurate and reproducible detection of proteins in water using an extended-gate type organic transistor biosensor. Appl. Phys. Lett. 404 (2014) 243703. https://doi.org/10.3390/s16122033

[83] H.-C. Chen, Y.-T. Chen, R.-Y. Tsai, M.-C. Chen, S.-L. Chen, M.-C. Xiao, C.-L. Chen, M.-Y. Hua, A sensitive and selective magnetic graphene composite-modified polycrystalline-silicon nanowire field-effect transistor for bladder cancer diagnosis, Biosensors and Bioelectronics. 66 (2015) 198–207. https://doi.org/10.1016/j.bios.2014.11.019.

[84] Y. Zhang, R. Chen, L. Xu, Y. Ning, S. Xie, G.-J. Zhang, Silicon Nanowire Biosensor for Highly Sensitive and Multiplexed Detection of Oral Squamous Cell Carcinoma Biomarkers in Saliva, Anal. Sci. 31 (2015) 73–78. https://doi.org/10.2116/analsci.31.73.

[85] A. Gao, N. Lu, Y. Wang, T. Li, Robust ultrasensitive tunneling-FET biosensor for point-of-care diagnostics, Sci Rep. 6 (2016) 22554. https://doi.org/10.1038/srep22554.

[86] G. Presnova, D. Presnov, V. Krupenin, V. Grigorenko, A. Trifonov, I. Andreeva, O. Ignatenko, A. Egorov, M. Rubtsova, Biosensor based on a silicon nanowire field-effect transistor functionalized by gold nanoparticles for the highly sensitive determination of prostate specific antigen, Biosensors and Bioelectronics. 88 (2017) 283–289. https://doi.org/10.1016/j.bios.2016.08.054.

[87] A. Gao, X. Yang, J. Tong, L. Zhou, Y. Wang, J. Zhao, H. Mao, T. Li, Multiplexed detection of lung cancer biomarkers in patients serum with CMOS-compatible silicon nanowire arrays, Biosensors and Bioelectronics. 91 (2017) 482–488. https://doi.org/10.1016/j.bios.2016.12.072.

[88] J.-H. Lee, E.-J. Chae, S. Park, J.-W. Choi, Label-free detection of γ-aminobutyric acid based on silicon nanowire biosensor, Nano Convergence. 6 (2019) 13. https://doi.org/10.1186/s40580-019-0184-3.

[89] S.-M. Chang, S. Palanisamy, T.-H. Wu, C.-Y. Chen, K.-H. Cheng, C.-Y. Lee, S.-S.F. Yuan, Y.-M. Wang, Utilization of silicon nanowire field-effect transistors for the detection of a cardiac biomarker, cardiac troponin I and their applications involving animal models, Sci Rep. 10 (2020) 22027. https://doi.org/10.1038/s41598-020-78829-7.

[90] M. Zverzhinetsky, V. Krivitsky, F. Patolsky, Direct whole blood analysis by the antigen-antibody chemically-delayed dissociation from nanosensors arrays, Biosensors and Bioelectronics. 170 (2020) 112658. https://doi.org/10.1016/j.bios.2020.112658.

[91] D. Rani, Y. Singh, M. Salker, X.T. Vu, S. Ingebrandt, V. Pachauri, Point-of-care-ready nanoscale ISFET arrays for sub-picomolar detection of cytokines in cell cultures, Anal Bioanal Chem. 412 (2020) 6777–6788. https://doi.org/10.1007/s00216-020-02820-4.

[92] C.-A. Vu, W.-Y. Chen, Y.-S. Yang, H.W.-H. Chan, Improved biomarker quantification of silicon nanowire field-effect transistor immunosensors with signal enhancement by RNA aptamer: Amyloid beta as a case study, Sensors and Actuators B: Chemical. 329 (2021) 129150. https://doi.org/10.1016/j.snb.2020.129150.

[93] C.-A. Vu, P.-H. Pan, Y.-S. Yang, H.W.-H. Chan, Y. Kumada, W.-Y. Chen, Combination of Aptamer Amplifier and Antigen-Binding Fragment Probe as a Novel Strategy to Improve Detection Limit of Silicon Nanowire Field-Effect Transistor Immunosensors, Sensors. 21 (2021) 650. https://doi.org/10.3390/s21020650.

[94] K.A. Malsagova, T.O. Pleshakova, A.F. Kozlov, R.A. Galiullin, V.P. Popov, F.V. Tikhonenko, A.V. Glukhov, V.S. Ziborov, I.D. Shumov, O.F. Petrov, V.M. Generalov, A.A. Cheremiskina, A.G. Durumanov, A.P. Agafonov, E.V. Gavrilova, R.A. Maksyutov, A.S. Safatov, V.G. Nikitaev, A.N. Pronichev, V.A. Konev, A.I. Archakov, Y.D. Ivanov, Detection of Influenza Virus Using a SOI-Nanoribbon Chip, Based on an N-Type Field-Effect Transistor, Biosensors. 11 (2021) 119. https://doi.org/10.3390/bios11040119.

[95] H. Park, S. Baek, B. Jeong, A. sen, S. Kim, Y.C. Park, S. Kim, young jun kim, Nanomesh-patterning on multilayer MoS2 field-effect transistors for ultra-sensitive detection of cortisol, (2020). https://doi.org/10.21203/rs.3.rs-64919/v1.

[96] N.R. Dalila, M.K.M. Arshad, S.C.B. Gopinath, M.N.M. Nuzaihan, M.F.M. Fathil, Molybdenum disulfide—gold nanoparticle nanocomposite in field-effect transistor back-gate for enhanced C-reactive protein detection, Microchim Acta. 187 (2020) 588. https://doi.org/10.1007/s00604-020-04562-7.

[97] M. Ma, L. Chao, Y. Zhao, J. Ding, Z. Huang, M. Long, F. Wang, J. Jiang, Z. Liu, High-sensitivity detection of Concanavalin A using MoS2-based field effect transistor biosensor, J. Phys. D: Appl. Phys. 54 (2021) 245401. https://doi.org/10.1088/1361-6463/abeeb9.

[98] Y. Zhang, D. Feng, Y. Xu, Z. Yin, W. Dou, U.E. Habiba, C. Pan, Z. Zhang, H. Mou, H. Deng, X. Mi, N. Dai, DNA-based functionalization of two-dimensional MoS2 FET biosensor for ultrasensitive detection of PSA, Applied Surface Science. 548 (2021) 149169. https://doi.org/10.1016/j.apsusc.2021.149169.

[99] B. Chakraborty, R. Saha, S. Chattopadhyay, D. De, R.D. Das, M.K. Mukhopadhyay, M. Palit, C. RoyChaudhuri, Impact of surface defects in electron beam evaporated ZnO thin films on FET biosensing characteristics towards reliable PSA detection, Applied Surface Science. 537 (2021) 147895. https://doi.org/10.1016/j.apsusc.2020.147895.

[100] H. Woo Son, J.H. Park, M.-S. Chae, B.-H. Kim, T.G. Kim, Bilayer indium gallium zinc oxide electrolyte-gated field-effect transistor for biosensor platform with high reliability, Sensors and Actuators B: Chemical. 312 (2020) 127955. https://doi.org/10.1016/j.snb.2020.127955.

[101] P. Song, H. Fu, Y. Wang, C. Chen, P. Ou, R.T. Rashid, S. Duan, J. Song, Z. Mi, X. Liu, A Microfluidic Field-Effect Transistor Biosensor with Rolled-Up Indium Nitride Microtubes, Biosensors and Bioelectronics. (2021) 113264. https://doi.org/10.1016/j.bios.2021.113264.

[102] N. Nakatsuka, J.M. Abendroth, K.-A. Yang, A.M. Andrews, Divalent Cation Dependence Enhances Dopamine Aptamer Biosensing, ACS Appl. Mater. Interfaces. 13 (2021) 9425–9435. https://doi.org/10.1021/acsami.0c17535.

[103] H. Chen, T.K. Choo, J. Huang, Y. Wang, Y. Liu, M. Platt, A. Palaniappan, B. Liedberg, A.I.Y. Tok, Label-free electronic detection of interleukin-6 using horizontally aligned carbon nanotubes, Materials & Design. 90 (2016) 852–857. https://doi.org/10.1016/j.matdes.2015.11.029.

[104] N. Belkhamssa, J.P. da Costa, C.I.L. Justino, P.S.M. Santos, S. Cardoso, A.C. Duarte, T. Rocha-Santos, M. Ksibi, Development of an electrochemical biosensor for alkylphenol detection, Talanta. 158 (2016) 30–34. https://doi.org/10.1016/j.talanta.2016.05.044.

[105] N. Belkhamssa, C.I.L. Justino, P.S.M. Santos, S. Cardoso, I. Lopes, A.C. Duarte, T. Rocha-Santos, M. Ksibi, Label-free disposable immunosensor for detection of atrazine, Talanta. 146 (2016) 430–434. https://doi.org/10.1016/j.talanta.2015.09.015.

[106] N.T. Tung, P.T. Tue, T. Thi Ngoc Lien, Y. Ohno, K. Maehashi, K. Matsumoto, K. Nishigaki, M. Biyani, Y. Takamura, Peptide aptamer-modified single-walled carbon nanotube-based transistors for high-performance biosensors, Sci Rep. 7 (2017) 17881. https://doi.org/10.1038/s41598-017-18169-1.

[107] V.A. Pham Ba, Y.M. Han, Y. Cho, T. Kim, B.Y. Lee, J.S. Kim, S. Hong, Modified Floating Electrode-Based Sensors for the Quantitative Monitoring of Drug Effects on Cytokine Levels Related with Inflammatory Bowel Diseases, ACS Appl. Mater. Interfaces. 10 (2018) 17100–17106. https://doi.org/10.1021/acsami.8b04287.

[108] M.S. Filipiak, M. Rother, N.M. Andoy, A.C. Knudsen, S. Grimm, C. Bachran, L.K. Swee, J. Zaumseil, A. Tarasov, Highly sensitive, selective and label-free protein detection in physiological solutions using carbon nanotube transistors with nanobody receptors, Sensors and Actuators B: Chemical. 255 (2018) 1507–1516. https://doi.org/10.1016/j.snb.2017.08.164.

[109] Y. Sun, Z. Peng, H. Li, Z. Wang, Y. Mu, G. Zhang, S. Chen, S. Liu, G. Wang, C. Liu, L. Sun, B. Man, C. Yang, Suspended CNT-Based FET sensor for ultrasensitive and label-free detection of DNA hybridization, Biosensors and Bioelectronics. 137 (2019) 255–262. https://doi.org/10.1016/j.bios.2019.04.054.

[110] S. G. Surya, S. M. Majhi, D. K. Agarwal, A. Ait Lahcen, S. Yuvaraja, K. N. Chappanda, K. N. Salama, A label-free aptasensor FET based on Au nanoparticle decorated Co 3 O 4 nanorods and a SWCNT layer for detection of cardiac troponin T protein, Journal of Materials Chemistry B. 8 (2020) 18–26. https://doi.org/10.1039/C9TB01989H.

[111] C.-H. Han, J. Jang, Integrated microfluidic platform with electrohydrodynamic focusing and a carbon-nanotube-based field-effect transistor immunosensor for continuous, selective, and label-free quantification of bacteria, Lab on a Chip. 21 (2021) 184–195. https://doi.org/10.1039/D0LC00783H.

[112] M. Thanihaichelvan, S.N. Surendran, T. Kumanan, U. Sutharsini, P. Ravirajan, R. Valluvan, T. Tharsika, Selective and electronic detection of COVID-19 (Coronavirus) using carbon nanotube field effect transistor-based biosensor: A proof-of-concept study, Materials Today: Proceedings. (2021). https://doi.org/10.1016/j.matpr.2021.05.011.

[113] M. Thanihaichelvan, L.A. Browning, M.P. Dierkes, R.M. Reyes, A.V. Kralicek, C. Carraher, C.A. Marlow, N.O.V. Plank, Metallic-semiconducting junctions create sensing hot-spots in carbon nanotube FET aptasensors near percolation. Biosensors and Bioelectronics 130 (2019) 408–413. https://doi.org/10.1016/j.bios.2018.09.021.

[114] G. Xu, J. Abbott, L. Qin, K.Y.M. Yeung, Y. Song, H. Yoon, J. Kong, D. Ham, Electrophoretic and field-effect graphene for all-electrical DNA array technology, Nat Commun. 5 (2014) 4866. https://doi.org/10.1038/ncomms5866.

[115] B. Cai, L. Huang, H. Zhang, Z. Sun, Z. Zhang, G.-J. Zhang, Gold nanoparticles-decorated graphene field-effect transistor biosensor for femtomolar MicroRNA detection, Biosensors and Bioelectronics. 74 (2015) 329–334. https://doi.org/10.1016/j.bios.2015.06.068.

[116] C. Zheng, L. Huang, H. Zhang, Z. Sun, Z. Zhang, G.-J. Zhang, Fabrication of Ultrasensitive Field-Effect Transistor DNA Biosensors by a Directional Transfer Technique Based on CVD-Grown Graphene, ACS Appl. Mater. Interfaces. 7 (2015) 16953–16959. https://doi.org/10.1021/acsami.5b03941.

[117] J. Basu, S. Datta, C. RoyChaudhuri, A graphene field effect capacitive Immunosensor for sub-femtomolar food toxin detection, Biosensors and Bioelectronics. 68 (2015) 544–549. https://doi.org/10.1016/j.bios.2015.01.046.

[118] S. Farid, X. Meshik, M. Choi, S. Mukherjee, Y. Lan, D. Parikh, S. Poduri, U. Baterdene, C.-E. Huang, Y.Y. Wang, P. Burke, M. Dutta, M.A. Stroscio, Detection of Interferon gamma using graphene and aptamer based FET-like electrochemical biosensor, Biosensors and Bioelectronics. 71 (2015) 294–299. https://doi.org/10.1016/j.bios.2015.04.047.

[119] J. Basu, C. RoyChaudhuri, Graphene Nanogrids FET Immunosensor: Signal to Noise Ratio Enhancement, Sensors. 16 (2016) 1481. https://doi.org/10.3390/s16101481.

[120] M.T. Hwang, P.B. Landon, J. Lee, D. Choi, A.H. Mo, G. Glinsky, R. Lal, Highly specific SNP detection using 2D graphene electronics and DNA strand displacement, PNAS. 113 (2016) 7088–7093.

[121] J. Ping, R. Vishnubhotla, A. Vrudhula, A.T.C. Johnson, Scalable Production of High-Sensitivity, Label-Free DNA Biosensors Based on Back-Gated Graphene Field Effect Transistors, ACS Nano. 10 (2016) 8700–8704. https://doi.org/10.1021/acsnano.6b04110.

[122] L. Zhou, H. Mao, C. Wu, L. Tang, Z. Wu, H. Sun, H. Zhang, H. Zhou, C. Jia, Q. Jin, X. Chen, J. Zhao, Label-free graphene biosensor targeting cancer molecules based on non-covalent modification, Biosensors and Bioelectronics. 87 (2017) 701–707. https://doi.org/10.1016/j.bios.2016.09.025.

[123] S. Xu, J. Zhan, B. Man, S. Jiang, W. Yue, S. Gao, C. Guo, H. Liu, Z. Li, J. Wang, Y. Zhou, Real-time reliable determination of binding kinetics of DNA hybridization using a multi-channel graphene biosensor, Nat Commun. 8 (2017) 14902. https://doi.org/10.1038/ncomms14902.

[124] A.K. Manoharan, S. Chinnathambi, R. Jayavel, N. Hanagata, Simplified detection of the hybridized DNA using a graphene field effect transistor, Science and Technology of Advanced Materials. 18 (2017) 43–50. https://doi.org/10.1080/14686996.2016.1253408.

[125] K. Islam, A. Suhail, G. Pan, A Label-Free and Ultrasensitive Immunosensor for Detection of Human Chorionic Gonadotrophin Based on Graphene FETs, Biosensors. 7 (2017) 27. https://doi.org/10.3390/bios7030027.

[126] B. Li, G. Pan, A. Suhail, K. Islam, N. Avent, P. Davey, Deep UV hardening of photoresist for shaping of graphene and lift-off fabrication of back-gated field effect biosensors by ion-milling and sputter deposition, Carbon. 118 (2017) 43–49. https://doi.org/10.1016/j.carbon.2017.03.032.

[127] Y. Yang, X. Yang, X. Zou, S. Wu, D. Wan, A. Cao, L. Liao, Q. Yuan, X. Duan, Ultrafine Graphene Nanomesh with Large On/Off Ratio for High-Performance Flexible Biosensors, Advanced Functional Materials. 27 (2017) 1604096. https://doi.org/10.1002/adfm.201604096.

[128] M. Tian, S. Xu, J. Zhang, X. Wang, Z. Li, H. Liu, R. Song, Z. Yu, J. Wang, RNA Detection Based on Graphene Field-Effect Transistor Biosensor, Advances in Condensed Matter Physics. 2018 (2018) 1–6. https://doi.org/10.1155/2018/8146765.

[129] N.N.M. Maidin, R.A. Rahim, N.H.A. Halim, A.S.Z. Abidin, N.A. Ahmad, Z. Lockman, Interaction of graphene electrolyte gate field-effect transistor for detection of cortisol biomarker, AIP Conference Proceedings. 2045 (2018) 020022. https://doi.org/10.1063/1.5080835.

[130] J. Antunes, C. Justino, J.P. da Costa, S. Cardoso, A.C. Duarte, T. Rocha-Santos, Graphene immunosensors for okadaic acid detection in seawater, Microchemical Journal. 138 (2018) 465–471. https://doi.org/10.1016/j.microc.2018.01.041.

[131] J. Basu, N. Samanta, S. Jana, C. RoyChaudhuri, Towards reliability enhancement of graphene FET biosensor in complex analyte: Artificial neural network approach, Microelectronics Reliability. 91 (2018) 154–159. https://doi.org/10.1016/j.microrel.2018.09.001.

[132] C. Haslam, S. Damiati, T. Whitley, P. Davey, E. Ifeachor, S.A. Awan, Label-Free Sensors Based on Graphene Field-Effect Transistors for the Detection of Human Chorionic Gonadotropin Cancer Risk Biomarker, Diagnostics. 8 (2018) 5. https://doi.org/10.3390/diagnostics8010005.

[133] S. Mansouri Majd, A. Salimi, Ultrasensitive flexible FET-type aptasensor for CA 125 cancer marker detection based on carboxylated multiwalled carbon nanotubes immobilized onto reduced graphene oxide film, Analytica Chimica Acta. 1000 (2018) 273–282. https://doi.org/10.1016/j.aca.2017.11.008.

[134] D.H. Kim, H.G. Oh, W.H. Park, D.C. Jeon, K.M. Lim, H.J. Kim, B.K. Jang, K.S. Song, Detection of Alpha-Fetoprotein in Hepatocellular Carcinoma Patient Plasma with Graphene Field-Effect Transistor, Sensors. 18 (2018) 4032. https://doi.org/10.3390/s18114032.

[135] N.M. Andoy, M.S. Filipiak, D. Vetter, Ó. Gutiérrez-Sanz, A. Tarasov, Graphene-Based Electronic Immunosensor with Femtomolar Detection Limit in Whole Serum, Advanced Materials Technologies. 3 (2018) 1800186. https://doi.org/10.1002/admt.201800186.

[136] R. Campos, J. Borme, J.R. Guerreiro, G. Machado, M.F. Cerqueira, D.Y. Petrovykh, P. Alpuim, Attomolar Label-Free Detection of DNA Hybridization with Electrolyte-Gated Graphene Field-Effect Transistors, ACS Sens. 4 (2019) 286–293. https://doi.org/10.1021/acssensors.8b00344.

[137] J. Sun, X. Xie, K. Xie, S. Xu, S. Jiang, J. Ren, Y. Zhao, H. Xu, J. Wang, W. Yue, Magnetic Graphene Field-Effect Transistor Biosensor for Single-Strand DNA Detection, Nanoscale Research Letters. 14 (2019) 248. https://doi.org/10.1186/s11671-019-3048-1.

[138] S. Islam, S. Shukla, V.K. Bajpai, Y.-K. Han, Y.S. Huh, A. Ghosh, S. Gandhi, Microfluidic-based graphene field effect transistor for femtomolar detection of chlorpyrifos, Sci Rep. 9 (2019) 276. https://doi.org/10.1038/s41598-018-36746-w.

[139] S. Islam, S. Shukla, V.K. Bajpai, Y.-K. Han, Y.S. Huh, A. Kumar, A. Ghosh, S. Gandhi, A smart nanosensor for the detection of human immunodeficiency virus and associated cardiovascular and arthritis diseases using functionalized graphene-based transistors, Biosensors and Bioelectronics. 126 (2019) 792–799. https://doi.org/10.1016/j.bios.2018.11.041.

[140] D. Kwong Hong Tsang, T.J. Lieberthal, C. Watts, I.E. Dunlop, S. Ramadan, A.E. del Rio Hernandez, N. Klein, Chemically Functionalised Graphene FET Biosensor for the Label-free Sensing of Exosomes, Sci Rep. 9 (2019) 13946. https://doi.org/10.1038/s41598-019-50412-9.

[141] R. Hajian, S. Balderston, T. Tran, T. deBoer, J. Etienne, M. Sandhu, N.A. Wauford, J.-Y. Chung, J. Nokes, M. Athaiya, J. Paredes, R. Peytavi, B. Goldsmith, N. Murthy, I.M. Conboy, K. Aran, Detection of unamplified target genes via CRISPR–Cas9 immobilized on a graphene field-effect transistor, Nat Biomed Eng. 3 (2019) 427–437. https://doi.org/10.1038/s41551-019-0371-x.

[142] Y. Kanai, Y. Ohmuro-Matsuyama, M. Tanioku, S. Ushiba, T. Ono, K. Inoue, T. Kitaguchi, M. Kimura, H. Ueda, K. Matsumoto, Graphene Field Effect Transistor-Based Immunosensor for Ultrasensitive Noncompetitive Detection of Small Antigens, ACS Sens. 5 (2020) 24–28. https://doi.org/10.1021/acssensors.9b02137.

[143] J.B. Pal, Detection of Biomolecules in High Ionic Strength physiological Solution Using Electrochemically Reduced Graphene oxide Field-Effect Transistor Immunosensor, (2020). https://wvvw.easychair.org/publications/preprint/p7mK (accessed June 17, 2021).

[144] C. Zhang, S. Cheng, K. Si, N. Wang, Y. Wang, P. Chen, H. Dong, W. Hu, All-covalently-implanted FETs with ultrahigh solvent resistibility and exceptional electrical stability, and their applications for liver cancer biomarker detection, Journal of Materials Chemistry C. 8 (2020) 7436–7446. https://doi.org/10.1039/D0TC01385D.

[145] S. Wang, M.Z. Hossain, K. Shinozuka, N. Shimizu, S. Kitada, T. Suzuki, R. Ichige, A. Kuwana, H. Kobayashi, Graphene field-effect transistor biosensor for detection of biotin with ultrahigh sensitivity and specificity, Biosensors and Bioelectronics. 165 (2020) 112363. https://doi.org/10.1016/j.bios.2020.112363.

[146] M.T. Hwang, M. Heiranian, Y. Kim, S. You, J. Leem, A. Taqieddin, V. Faramarzi, Y. Jing, I. Park, A.M. van der Zande, S. Nam, N.R. Aluru, R. Bashir, Ultrasensitive detection of nucleic acids using deformed graphene channel field effect biosensors, Nat Commun. 11 (2020) 1543. https://doi.org/10.1038/s41467-020-15330-9.

[147] T. Bungon, C. Haslam, S. Damiati, B. O'Driscoll, T. Whitley, P. Davey, G. Siligardi, J. Charmet, S.A. Awan, Graphene FET Sensors for Alzheimer's Disease Protein Biomarker Clusterin Detection, Proceedings. 60 (2020) 14. https://doi.org/10.3390/IECB2020-07229.

[148] A. Roberts, N. Chauhan, S. Islam, S. Mahari, B. Ghawri, R.K. Gandham, S.S. Majumdar, A. Ghosh, S. Gandhi, Graphene functionalized field-effect transistors for ultrasensitive detection of Japanese encephalitis and Avian influenza virus, Sci Rep. 10 (2020) 14546. https://doi.org/10.1038/s41598-020-71591-w.

[149] A. Gaurav, P. Shukla, Rapid detection of covid-19 causative virus (sars-cov-2) using FET-based biosensor, Int Res J Modernizat Eng Technol Sci. 2 (2020) 1207–1214.

[150] Y. Xia, Y. Sun, H. Li, S. Chen, T. Zhu, G. Wang, B. Man, J. Pan, C. Yang, Plasma treated graphene FET sensor for the DNA hybridization detection, Talanta. 223 (2021) 121766. https://doi.org/10.1016/j.talanta.2020.121766.

[151] M.M. Nur Nasyifa, A.R. Ruslinda, N.H. Abdul Halim, A.S. Zainol Abidin, F.N. Mohd Faudzi, N.A. Ahmad, Z. Lockman, B. Rezek, A. Kromka, S.C.B. Gopinath, Immuno-probed graphene nanoplatelets on electrolyte-gated field-effect transistor for stable cortisol quantification in serum, Journal of the Taiwan Institute of Chemical Engineers. 117 (2020) 10–18. https://doi.org/10.1016/j.jtice.2020.12.008.

[152] S. Papamatthaiou, P. Estrela, D. Moschou, Printable graphene BioFETs for DNA quantification in Lab-on-PCB microsystems, Sci Rep. 11 (2021) 9815. https://doi.org/10.1038/s41598-021-89367-1.

[153] N. Mandal, V. Pakira, N. Samanta, N. Das, S. Chakraborty, B. Pramanick, C. RoyChaudhuri, PSA detection using label free graphene FET with coplanar electrodes based microfluidic point of care diagnostic device, Talanta. 222 (2021) 121581. https://doi.org/10.1016/j.talanta.2020.121581.

[154] J. Li, D. Wu, Y. Yu, T. Li, K. Li, M.-M. Xiao, Y. Li, Z.-Y. Zhang, G.-J. Zhang, Rapid and unamplified identification of COVID-19 with morpholino-modified graphene field-effect transistor nanosensor, Biosensors and Bioelectronics. 183 (2021) 113206. https://doi.org/10.1016/j.bios.2021.113206.

[155] S.J. Park, S.E. Seo, K.H. Kim, S.H. Lee, J. Kim, S. Ha, H.S. Song, S.H. Lee, O.S. Kwon, Real-time monitoring of geosmin based on an aptamer-conjugated graphene field-effect transistor, Biosensors and Bioelectronics. 174 (2021) 112804. https://doi.org/10.1016/j.bios.2020.112804.

[156] P. Aspermair, V. Mishyn, J. Bintinger, H. Happy, K. Bagga, P. Subramanian, W. Knoll, R. Boukherroub, S. Szunerits, Reduced graphene oxide–based field effect transistors for the detection of E7 protein of human papillomavirus in saliva, Anal Bioanal Chem. 413 (2021) 779–787. https://doi.org/10.1007/s00216-020-02879-z.

[157] S. Xu, T. Wang, G. Liu, Z. Cao, L.A. Frank, S. Jiang, C. Zhang, Z. Li, V.V. Krasitskaya, Q. Li, Y. Sha, X. Zhang, H. Liu, J. Wang, Analysis of interactions between proteins and small-molecule drugs by a biosensor based on a graphene field-effect transistor, Sensors and Actuators B: Chemical. 326 (2021) 128991. https://doi.org/10.1016/j.snb.2020.128991.

[158] I. Novodchuk, M. Kayaharman, I.R. Ausri, R. Karimi, X.S. Tang, I.A. Goldthorpe, E. Abdel-Rahman, J. Sanderson, M. Bajcsy, M. Yavuz, An ultrasensitive heart-failure BNP biosensor using B/N co-doped graphene oxide gel FET, Biosensors and Bioelectronics. 180 (2021) 113114. https://doi.org/10.1016/j.bios.2021.113114.

[159] Y. Zhang, Y. Ding, C. Li, H. Xu, C. Liu, J. Wang, Y. Ma, J. Ren, Y. Zhao, W. Yue, An optic-fiber graphene field effect transistor biosensor for the detection of single-stranded DNA, Analytical Methods. 13 (2021) 1839–1846. https://doi.org/10.1039/D1AY00101A.

[160] S. Ramadan, R. Lobo, Y. Zhang, L. Xu, O. Shaforost, D. Kwong Hong Tsang, J. Feng, T. Yin, M. Qiao, A. Rajeshirke, L.R. Jiao, P.K. Petrov, I.E. Dunlop, M.-M. Titirici, N. Klein, Carbon-Dot-Enhanced Graphene Field-Effect Transistors for Ultrasensitive Detection of Exosomes, ACS Appl. Mater. Interfaces. 13 (2021) 7854–7864. https://doi.org/10.1021/acsami.0c18293.

[161] T. Bungon, C. Haslam, S. Damiati, B. O'Driscoll, T. Whitley, P. Davey, G. Siligardi, J. Charmet, S.A. Awan, Graphene FET Sensors for Alzheimer's Disease Protein Biomarker Clusterin Detection, Front Mol Biosci. 8 (2021) 651232. https://doi.org/10.3389/fmolb.2021.651232.

[162] Z. Wang, Z. Hao, X. Wang, C. Huang, Q. Lin, X. Zhao, Y. Pan, A Flexible and Regenerative Aptameric Graphene–Nafion Biosensor for Cytokine Storm Biomarker Monitoring in Undiluted Biofluids toward Wearable Applications, Advanced Functional Materials. 31 (2021) 2005958. https://doi.org/10.1002/adfm.202005958.

[163] S. Balderston, J.J. Taulbee, E. Celaya, K. Fung, A. Jiao, K. Smith, R. Hajian, G. Gasiunas, S. Kutanovas, D. Kim, J. Parkinson, K. Dickerson, J.-J. Ripoll, R. Peytavi, H.-W. Lu, F. Barron, B.R. Goldsmith, P.G. Collins, I.M. Conboy, V. Siksnys, K. Aran, Discrimination of single-point mutations in unamplified genomic DNA via Cas9 immobilized on a graphene field-effect transistor, Nat Biomed Eng. (2021) 1–13. https://doi.org/10.1038/s41551-021-00706-z.

[164] S. Sheibani, L. Capua, S. Kamaei, S.S.A. Akbari, J. Zhang, H. Guerin, A.M. Ionescu, Extended gate field-effect-transistor for sensing cortisol stress hormone, Commun Mater. 2 (2021) 1–10. https://doi.org/10.1038/s43246-020-00114-x.

[165] K. Shoorideh, C.O. Chui. On the origin of enhanced sensitivity in nanoscale FET-based biosensors. PNAS 2014;111:5111–6. https://doi.org/10.1073/pnas.1315485111.

Table 1. Silicon-based field-effect transistors for affinity sensing

Target	Receptor functionalization	FET Structure	Detection Technique	Detection limit (LOD)	Dynamic range	Ref
Liquid gated silicon-based FET						
CYFRA 21-1	Anti- CYFRA 21-1-antibody (APTES/glutaraldehyde: covalent binding)	Si substrate, SiO_2-gate FETs, size of each gate insulator L x W (10 µm × 1000 µm)	Electrical measurement: ΔVg vs [CYFRA 21-1]/[NSE]	1 ng/mL	1-1000 ng/mL	[49]
NSE	Anti- NSE-antibody (APTES/glutaraldehyde: covalent binding)			10 ng/mL (PBS) 100 ng/mL (HS)		
IL-5	Anti-human IL-5 APTMS/succinic anhydride/EDC-NHS: Covalent binding ALP labeled Ab	SiO_2 gate FET, Al (150 nm) electrodes, channel L/W (10/10 µm)	Electrical measurement: I_{DS} vs V_g I_{DS} vs V_{DS} ΔV_R vs Time	1 ng/mL	1 pg/mL-10 ng/mL	[50]
H1N1 human IFV	Glycan (AOPTES: covalent binding)	SiO_2 substrate, Each FET had two channels, gate size L x W L 10µm × 1000µm	Electrical measurement: ΔVg vs [IFV]	$10^{0.5}$ $TCID_{50}$/mL	$10^{0.5}$ to $10^{8.5}$ $TCID_{50}$/mL	[51]
H5N1 avian IFV	Glycan (AOPTES: covalent binding)					

Cortisol	Aptamer (APTES/glutaraldehyde: covalent binding)	SiO_2 gate n-type FET Channel L/W (10/1 µm)	Electrical measurement: ΔV_g vs [cortisol]	50 µmol/L	50-1000µmol/L	[52]
3-nitrotyrosine (3-NT)	Anti-3-NT-antibody (APTES: Covalent binding)	Si_3N_4/SiO_2 gate FET	Electrical measurement: G_{pc} vs [3-NT]	0.15 ng/mL 10 ng/mL (LOQ)	10 ng/mL-1000 ng/mL	[53]
TNF-α	Anti-TNF-α antibody (TESUD: Covalent binding)	Si_3N_4/SiO_2 gate FET Ti/Pt (15/150 nm) electrodes, gate area dimensions 400 × 20 µm	Electrical measurement: I_{DS} vs V_{DS} I_{DS} vs V_{DS} G_m vs V_{GS}	5 pg/mL	5 pg/mL-20 pg/mL	[54]
TNF-α	Anti-cortisol antibody (TESUD: Covalent binding)	Si_3N_4/SiO_2 gate FET Ti/Pt (15/150 nm) electrodes, gate area dimensions 400 × 20 µm	EIS	1 pg/mL	1 pg/mL-50 pg/mL	[55]
Extended gated silicon based FETs						
DNA	PNA probe (Covalent binding)	MOSFET Au electrodes with a Ø 2.5mm as extended sensing electrode	Electrical measurement: Potentiel change vs [DNA]	1µM	10 nM-1 µM	[56]
TSH	anti-TSH antibody (EDC/NHS: covalent binding)	MOSFET, Ti/Au (10/100nm) electrodes onto glass slides (dimensions 1.5 mm × 0.75 mm), Extended gate	Electrical measurement: ΔV vs [TSH] ΔV vs Time	100 fM	300 fM- 10 nM	[57]
tumour suppressor p53	mouse monoclonal anti-p53 (PEG/EDC/NHS: covalent binding)	MOSFET, gold extended gate (sensing area 20 mm^2)	Electrical measurement: I_{DS} vs V_{ref} I_{DS} vs time ΔV_{TH} vs [p53]	100 pM 1.5 mV/dec (S)	0.1 -10 nM	[58]

Tau protein	Anti-tau IgG mouse monoclonal HT7 antibody (PEG/EDC/NHS: covalent binding)	MOSFET, gold extended gate	QCM measurement Differential readout	1 pM (buffer/ CCM) 10 pM (A-CSF)	1 pM- 10 nM	[59]
C-RP	Monoclonal anti-C-RP antibody (TPGA/EDC/NHS: covalent binding)	enEDL-FET	Electrical measurement: I_{DS} vs V_{GS} G_m VS V_{GS} ΔI_d vs [C-RP] ΔV_g vs [C-RP] Impedance	0.5 mg/L	0.5-5 mg/L	[60]

A-CSF: Artificial-Tau protein in cerebrospinal fluid; AOPTES: 3-aminooxypropyltriethoxy-silane; APTES: 3-aminopropyl triethoxysilane; CCM: cell culture media; FTO: Fluorine-doped tin oxide; G_{pc}: gate potential change; GPTES: (3-glycidyloxypropyl) triethoxysilane; IFV: avian infuenza virus; MCH: 6-mercapto-1-hexanol; PANI: polyaniline; TSH: thyroid stimulating hormone; TPGA: thiol-polyethylene glycol-amine; S_I: current sensitivity; ssDNA: thiolated bio-receptor single-strand DNA

Table 2. AlGaN/GaN High Electron Mobility Transistors for affinity sensing

Target	Receptor functionalization	FET Structure	Detection Technique	Detection limit (LOD)	Dynamic range	Ref
C-RP	monoclonal anti-C-RP antibody produced in mice (MUA/EDC/NHS: covalent binding)	MOCVD AlGaN/GaN, Sapphire substrate, Ni/Au gate, Si/Ti/Al/Ni/Au (1/25/160/40/100 nm) electrodes, gate L/W (20/200 µm)	Electrical measurement: I_{DS} vs V_{GS} I_{DS} vs V_{DS} ΔV_{out} vs [C-RP]	10 ng/mL	10 ng/mL-1000 ng/mL	[61]
DNA	DNA probe (TFAAD: covalent binding)	MOCVD AlGaN/GaN, SiC substrate, Al/Ti/Au electrodes, electrolyte-gated	Electrical measurement: I_{DS} vs [DNA] ΔU_{thr} vs [DNA] ΔI_{DS} vs [DNA]	10^{-14} M	10^{-16}-10^{-6} M	[62]
HIV-1 RT	Thiolated ssDNA aptamer (strong S-Au covalent binding)	MBE AlGaN/GaN, silicon substrate, ohmic contacts (60×60µm^2) of source/drain metals (gap 30µm/ channel W 50µm), 1200Å Au layer forms the metal interconnects and the gate electrode, gap between the openings/gate electrode /transistor channel (65/ 265/465µm	Electrical measurement: I_{DS} vs Time I_{DS} vs V_{DS} TC vs [HIV-1 RT]/[CEA]/[NT-proBNP]/[C-RP]	1 fM	1 fM-10 pM	[63]
CEA	Anti-CEA- Antibody (strong S-Au covalent binding)			100 fM	100 fM-1 nM	
NT-proBNP	Anti-NT-proBNP antibody (strong S-Au covalent binding)			100 fM	100 fM-1 nM (PBS) 180.9-5000 pg/mL (HS)	
C-RP	Aptamer (strong S-Au covalent binding)			1 fM	1 fM-100 nM (PBS) 0.34-23.2 mg/mL (HS)	

Zika virus	Zika antibody	AlGaN/GaN grown on sapphire substrate, two 100 µm wide metal lines of Ni/Au (20 nm/80 nm) separated by 20 µm, contact window 100 µm x 100 µm	Electrical measurement: I_d vs time I_d vs [Zika]	0.1 ng/mL	0.1-100 ng/mL	[64]
PSA	Anti-PSA antibody (glutaraldehyde: covalent binding)	MOCVD AlGaN (18 nm)/GaN (1.5µm), Si substrate, Ohmic contacts dimensions of 2.2 × 2.2 mm^2 (gaps of 2 mm by deposition Ti/Al/Ni/Au), Ti/Ni/Au source/drain	Electrical measurement: I_{DS} vs V_{DS} I_{DS} vs time $\Delta I/I_0$ vs [PSA]	100 fg/mL	100 fg/mL-100 ng/mL	[65]
NT-proBNP	Aptamer (adsorption)	MOCVD AlGaN/GaN, Si substrate, Ti/Al/ Ni/Au (200/400/800/1000 Å) electrodes	Electrical measurement: Gain vs [NT-proBNP] I_d vs time V_g vs [NT-proBNP]	- 80.54 mV/dec (S)	0 -10 ng/mL	[66]
MIG	Anti-MIG	MOCVD AlGaN/GaN, Si substrate, Ni/Au (20/70 nm) gate (L 3µm), Ti/Al/Ni/Au (20/120/30/40 nm) source/drain	Electrical measurement : I_{DS} vs V_{DS} g_d vs V_{DS} g_d/I_{DS} vs V_{DS}	0.48 mA/µg mL^{-1} (S)	0.2 ng/mL-400 ng/mL	[67]
C-erbB-2	Anti-erbB-2			0.054mA/µg mL^{-1} (S)	4 µg/mL-13 µg/mL	
KIM-1	Anti-KIM-1			0.254 mA/µg mL^{-1} (S)	1 ng/mL- 7 ng/mL	
PSA	Anti-PSA			0.91 mA/µg mL^{-1} (S)	1 ng/mL-10 ng/mL	
Cortisol	Monoclonal antibody cortisol (DTSP: covalent binding)			1 pM	1 pM-1 nM	[68]

PSA	bio anti-PSA) (streptavidin/ biotinylated-urease: covalent binding)	MOCVD AlGaN (18 nm)/GaN (1.5 µm), sapphire substrate	Electrical measurement: I_{ds} vs V_{ds} I-I_0 vs time I-I_0 vs log [PSA]	1 fg/mL 3.73 µA/dec (S)	1 fg/mL-1 pg/mL	[69]

APTES: 3-aminopropyltriethoxysilane; bio anti-PSA: Biotinylated prostate specific antibody; C-RP: C-reactive protein; CEA: Carcinoembryonic Antigen; DTSP: 3,3'-dithiodipropionic acid di (N-hydroxysuccinimide ester); GOx: glucose oxidase; HIV-1 RT: Human Immunodeficiency Virus-1 Reverse Transcriptase; KIM-1: Kidney injury Molecule; MOCVD: metal-organic chemical vapor deposition; MUA: 11-mercaptoundecanoic acid; MIG: Monokine Induced by Interferon Gamma; MBE: molecular beam epitaxy; NT-proBNP: N-terminal pro b-type natriuretic peptide; TFAAD: 10-trifluoroacetamide-1-decene.

Table 3. Organic Field effect transistors for affinity sensing

Target	Receptor functionalization	FET Structure	Detection Technique	Detection limit (LOD)	Dynamic range	Ref
CR-P	anti- CR-P antibody SA(AV)/Ab	EGOFET P3HT as OSC PL layer on OSC film		1 µg/mL in serum		[70]
Human Glycoprotein (CgA)	Anti CgA antibody (biotin: covalent binding) On gold extended gate	Extended gate OFET PBTT as OSC Al gate electrode deposited on a glass substrate (30 nm), gate dielectric consists of a thin-film of aluminum oxide layer (AlOx, 5 nm) and a C14-PA, 1.7 nm), Au 30 nm electrodes, channel W/L (500/20 µm	Electrical measurement: I_{DS} vs V_{GS} V_{TH} vs [CgA]	PBS 0.31 µg/mL (LOQ: 1.0 µg/mL) AS 0.11 µg/mL (LOQ : 0.38 µg/mL)	1 µg/mL-50 µg/mL	[71]
CR-P	Monoclonal anti- CR-P antibody	EGOFET P3HT as OSC	Electrical measurement: I_{DS} vs V_{DS}	2 pM (220 ng/L)	4 pM- 2 µM)	

	(P3HT: physical adsorption)	Si/SiO_2 substrate, Au IDE electrodes (10-µm channel length and 10-mm channel width), electrolyte-gated	I_{DS} vs V_g $\Delta I/I_0$ vs [CR-P]			[72]
PCT	Monoclonal anti-PCT antibody (P3HT: physical adsorption)	EGOFET P3HT as OSC Si/SiO_2 substrate, Au IDE electrodes (10 µm channel length and 10 mm channel width), electrolyte-gated	Electrical measurement: I_{DS} vs V_{DS} I_{DS} vs V_{GS} V_{TH} vs [PCT]	2.2 pM	0.8 pM-4.7 nM (PBS) 10 pg/mL-6000 pg/mL(MP)	[73]
GFAP	Anti-GFAP antibody PS-MA/NHS/EDC Covalent binding Embedded in PEG	Extended solution gate OFET Pentacene as OSC Interdigitated gold electrodes deposited on pentacene film on Si substrate	Electrical measurement: Drain current change	1.0 ng/mL	0.5 – 100 ng/mL	[74]
Cortisol	Anti-cortisol antibody (adsorption) Embedded in poly(styrene-co methacrylic acid	Extended gate EGOFET Pentacene as OSC ITO/poly(ethylene terephthalate) substrate, flexible electrodes, sensing membrane PSMA deposited on the gate surface	Electrical measurement: I_{DS} vs V_g $\Delta V_R/V_{base}$ vs [cortisol] $\Delta V_R/V_{base}$ vs Time	PBS 1 pg/mL Artificial sweat 1 ng/mL 10fg/mL-10 ng/mL (S)	1 fg/mL-100 pg/mL	[75]
Cortisol	Cortisol aptamer (UV immobilization)	OEGFET TIPS pentacene as OSC Cr electrode, transistor cluster consists of the devices with channel L (15–30 µm)/ AR (20–60), electrolyte-gated	Electrical measurement: I_{DS} vs V_{DS} G_m vs [cortisol]	27.3 pM	27.3 pM-27.3 µM	[76]
Anti-drug antibodies (ADAs)	Anti-Nivolumab (Cys-protein G: covalent binding) On gate electrode	EGOFET TIPS-pentacene as OSC TIPS Quartz substrate, Au gate, IDE Au electrodes (width-to-length ratio W/L = 500), electrolyte-gated	Electrical measurement: I_{DS} vs V_{GS} EIS	100 fM 1 x 10^{11} M^{-1} at 1 pM ADA (S)	1 pM-10 nM	[77]

Herbicides (glyphosate, diuron)	Aliginate hydrogel With immobilized algea	EGOFET Poly(DPP-DTT) as p-tyep OSC Pt gate microelectrode	Electrical measurement: I_{DS} vs V_{DS} I_{DS} vs V_{GS}	10 µM-	-	[78]
AFP	Anti-AFP (BFPA: covalent binding)	PDVT as organic thin film OSC Si/SiO_2 substrate, Au (30 nm) electrodes Back gated	Electrical measurement: I_{DS} vs V_g I_{DS} vs V_{DS} ΔI_{DS} vs [AFP]	45 fM for I_{DS} 53 fM for V_{TH}	10^{-2} ng/mL-10^3 ng/mL	[79]
IgG	biotinylated polyclonal antibody (Biotin/Streptavidin: covalent binding)	double gate FET diF-TES-ADT as OSC Parylene substrate, Ag electrode, dual gate, Ag/c-PVP bottom gate, Au/parylene top-gate	Electrical measurement: ΔV_{TH} vs [IgG] I_{DS} vs V_{BG} ΔV_{TH} vs V_{TG}	-	0 µg/mL-80 µg/mL	[80]
DNA	ssDNA (MCH: co-immobilization)	Extended gate FET PANI thin films as OSC Au electrodes, extended gate	EIS	9.77 pM	1 pM-1µM	[81]

AS: Artificial saliva; Al: aluminum; AR: aspect ratios; AFP: alpha-fetoprotein; Ag: Silver; BFPA: 2,6-bis(4- formylphenyl)anthracene; C14-PA: tetradecylphosphonic acid; Cr: chrome; c-PVP: poly(4-vinylphenol); diF-TES—ADT 2,8-difluoro-5,11-bis(triethylsilylethynyl)anthradithiophene; EIS: Electrochimical impedance spectroscopy; GFAP: glial fibrillary acidic protein; ITO: Indium–tin oxide; PBTTT: poly(2,5-bis(3-hexadecylthiophene-2-yl)thieno[3,2-*b*]thiophene; poly(DPP-DTT): poly(N-alkyldiketopyrrole dithienylthienol[3,2-*b*]thiophene; P3HT: poly-3-hexyl thiophene; PCT: procalcitonin; PSMA: poly(styrene-co-methacrylic acid); TIPS-pentacene: 6,13-bis(triisopropylsilylethinyl)pentacene; V_{TH}: threshold voltage; V_{TG} : top-gate terminal; V_{BG}: bottom-gate terminal

Table 4. Silicon nanowire field-effect transistors for affinity sensing

Target	Receptor functionalization	FET Structure	Detection Technique	Detection limit (LOD)	Dynamic range	Ref
APOA2 protein	Anti- APOA2 antibody Immobilized on magnetic graphene	Top-down approach CMOS process p-type SiNW	Electrical measurement: I_{DS} vs V_g $\Delta I/I_0$ vs [APOA2]	6.7 pg/mL	19.5 pg/mL-1.95 µg/mL	[83]
IL-8	Anti-human IL-8 (APTES/glutaraldehyde : covalent binding)	Top-down approach SOI substrate (700 nm silicon/145 nm buried oxide), SiNWs 90 µm long with 2 µm spacing in between 2 wires.	Electrical measurement: Resistance vs [TNF-α]/[IL-8]	10 fg/mL (PBS) 100 fg/mL (AS)	1fg/mL-1 ng/mL	[84]
TNF-α	Anti-human TNF-α (APTES/glutaraldehyde : covalent binding)					
CYFRA21-1	anti-CYFRA21-1-antibody (APTES/glutaraldehyde : covalent binding)	Top-down approach CMOS process SiNW length 16 µm ion implantation for source/drain (phosphor/boron) and intrinsic SiNW channel, Cr/Au on top of silicon contact	Electrical measurement: I_{DS} vs V_{GS} I_{DS} vs V_{DS} I_{DS} vs Time $\Delta I_{DS}/I_0$ vs [CYFRA21-1]	0.5 fg/mL (12.5 aM) 37 mV/dec (S)	0.5 fg/mL-10 ng/mL	[85]
PSA	Monoclonal anti-PSA antibody (covalent biding)	Top-down approach SOI wafer NW channel L/W of 3 mm/ 100 nm Ti/Si contacts	Electrical measurement: $I-I_0$ vs [PSA] $I-I_0/I_0$ vs Time	23 fg/mL	23 fg/mL-500 ng/mL	[86]
microRNA-126	DNA probe APTES/glutaraldehyde : covalent binding)	n-type SiNWs were 'topdown' fabricated with a CMOS, size from 20 to 200 nm, length vary from a few to 100 µm	Electrical measurement: I_{DS} vs Time $\Delta I_{DS}/I_0$ vs [miRNA]/[CEA]	0.1 fM	10^{-16} M-10^{-11} M	[87]
CEA	Anti-CEA			1 fg/mL (5.5 aM)	10^{-15} M-10^{-9} M	

	APTES/glutaraldehyde : covalent binding)					
GABA	Monoclonal antibody-GABA (TESBA: covalent binding)	Top-down approach SOI wafer 100 nm zig-zag shaped p-type silicon nanowire was fabricated on SOI wafer, Cr/Au (150, 30 nm) electrodes	Electrical measurement: I_{DS} vs V_{DS} I_{DS} vs V_g G vs Time G vs Log [GABA]	970 fM	970 fM-9.7 µM	[88]
cTnI	Monoclonal cTnI (APTES/glutaraldehyde : covalent binding)	Top-down approach SOI wafer diameter/ thickness (150±0.5 mm, 675±25 µm), H-wet-oxide and H-nitride oxidative layers with a 300 Å thickness were coated on top of SOI wafer to form an oxidation layer	Electrical measurement: I_{DS} vs Time $\Delta A/A_0$ vs [cTnI]	0.016 ng/mL	0.025 ng/mL-0.5 ng/mL	[89]
CTnT	Anti-Troponin T	Bottom-up approach VLS-CVD SiNW on Si(100) substrate Ti/Pd/Ti electrodes -	analysis of the 'dissociation regime' for any antibody- antigen pair	100 fM	100fM-100 pM	[90]
cTnI	Anti-Troponin I					
IL-4	Anti-IL-4 antibody (GPTES: Covalent binding)	Nano ISFET top-down lithography process, SOI substrate, Si NWs L/W/H (14 µm/250 nm/60 nm)	Electrical measurement: I_{DS} vs V_g V_{TH} vs I_{DS} vs Time	3-5 fM	25 fg/mL(1.92 fM)-2.5µg/mL(192 nM)	[91]
IL-2	Anti-IL-2 antibody (GPTES: Covalent binding)					
Amyloid beta (Aβ)1-42	Mouse anti-Aβ Antibody (APTES/glutaraldehyde : covalent binding)	Top-down approach two nanowire channels with dimensions L/W (2 µm/200 nm)	Electrical measurement: Voltage shift vs [Aβ1-42]	100 fg/mL (HS) 1 pg/mL	10^{-1}-pg/mL-10^{2} pg/mL (HS) 1-pg/mL-10^{3} pg/mL (BTP)	[92]

				(BTP)		
IgG	Fab anti-IgG (APTES/glutaraldehyde : covalent binding) Mixed with PEG Enhancement by R18 aptamer	Top-down approach two nanowire channels with dimensions L/W (2 µm/200 nm) -	Electrical measurement: I_{DS} vs V_g Voltage shift vs [IgG]	1 pg/mL	1 pg/mL-1 ng/mL	[93]
Influenza A	Antibodies against the influenza A virus (subtype A (H1N1) pdm09) (APTES/DTSSP: covalent binding)	Top-down approach on SOI Si Nanoribbon, poly Si electrodes, back gated	Electrical measurement, NR detector	6 10^{-16} M (10^4 VP/mL)	10^7- 10^3 VP/mL	[94]

AS: Artificial saliva; APOA2 protein: apolipoprotein A II protein; HS: human serum; BTP: Bis-Tris Propane; cTnT: cardiac troponin T; cTnI: cardiac Troponin I; CMOS: complementary metal oxide semiconductor; GABA: γ-Aminobutyric acid; G: conductance; PSA: prostate specific antigen; IgG: Immunoglobulin G; miRNA: microRNA; SOI: silicon-on-insulator; TESBA: Tri-ethoxy-silylbutyl-aldehyde.

Table 5. Other inorganic nanomaterials – based field effect transistors for the affinity sensing

Target	Receptor functionalization	FET Structure	Detection Technique	Detection limit (LOD)	Dynamic range	Ref
			MoS_2			
Cortisol	Aptamer cortisol (APTES/glutaraldehyde: covalent binding)	Exfoliated MoS_2, Si/SiO_2 substrate, Ti 20 nm/Au 100 nm electrodes	Electrical measurement: I_{DS} vs V_{GS} I_{DS} vs V_{DS}	10^{-18} g/mL	10^{-18} g/mL- 10^{-13} g/mL	[95]

			Sensitivity vs [Cortisol]			
C-RP	C-RP antibody (APTES/EDC/NHS/16-MDA: covalent binding)	MoS_2 grown on Si/SiO_2 substrate, Au/Ni Source/Drain, back-gated	Electrical measurement: I_{DS} vs VDS	8.38 fg/mL 176 nA/g.mL^{-1} (Sensitivity)	100 fg/mL-10 ng/mL	[96]
ConA	D-manose (MEA: covalent binding)	MoS_2 grown on Si/SiO_2 substrate, Ni (30 nm) electrodes	Electrical measurement: I_{DS} vs V_g I_{DS} vs V_{DS} $\Delta G/G_0$ vs [ConA]	105 nM	1×10^{-7} M – 1×10^{-3} M	[97]
PSA	Anti-PSA (biotin-streptavidin: Covalent binding)	Exfoliated MoS_2 (3-20nm), Si/SiO_2 substrate, Cr/Au (15/75 nm) source/drain, back-gated	Electrical measurement: I_{DS} vs V_{DS} I_{DS} vs V_g I_{DS} vs Time $\Delta I/I_0$ vs [PSA]	1 fg/mL	1 fg/mL-100 ng/Ml	[98]
ZnO						
PSA	Anti-PSA antibody (MTS/GMBS: covalent binding)	Electron gun technique ZnO, glass substrate, Cr/Au (20/100 nm) electrodes L/W/spacing between the electrodes (154/8/15 µm), liquid gate	Electrical measurement: I_{DS} vs V_{GS} I_{DS} vs Time I_{DS} vs [PSA]	0.06 fM	0.06 fM-1000 fM	[99]
Streptavidin	Biotin (APTES: covalent binding)	RF IGZO (40-nm), Si/SiO_2 substrate, Mo (100 nm) electrodes, electrolyte gated	Electrical measurement: I_{DS} vs V_{DS} I_{DS} vs V_g ΔV_g vs time	1 pg/mL	1 pg/mL-100 ng/mL	[100]
InN						

HIV	HIV gp41 antibodies (APTMS/glutaraldehyde: covalent binding)	SiOx/SiNx on Si substrate/Al coating, deposition of sputtered InN, Ti/Au electrode	Electrical measurement: I_{DS} vs V_g I_{DS} vs [HIV] EIS	2.5 pM (0.1 ng/mL)	0.1 ng/mL-400 ng/mL	[101]
In_2O_3						
Dopamine	Aptamer (APTMS/PTMS/MBS: covalent binding)	In_2O_3 (4 nm) grown on Si/SiO_2 substrate, IDE Ti/Au (10/30 nm) electrodes W/L (80/1500 µm), liquid gate	Electrical measurement: I_{DS} vs V_{GS}	10 fM	10 fM-100 µM	[102]

CR-P: C-reactive protein; ConA: Concanavalin A; GMBS: N-γ-Maleimidobutyryloxysuccinimide; MEA: β-mercaptoethylamine; MTS: 3-mercaptopropyltrimethoxysilane; MoS_2: molybdenum disulde; 16-MDA: 16- mercaptohexadecanoic acid; Ni: Nickel; PSA: prostate-specific antigen.

Table 6. Carbon nanotube field-effect transistors for affinity sensing.

Target	Receptor functionalization	FET Structure	Detection Technique	Detection limit (LOD)	Dynamic range	Ref
Interleukin-6	Antibody-IL-6R (PBASE: Covalent binding)	CVD SWCNT, Quartz substrate, 2 mm wide, 100 nm thick Au source and drain electrodes (spacing = 200 µm). Liquid gated	Electrical measurement: I_{DS} vs V_g I_{DS} vs V_D I_{DS} vs [IL-6]	1.37 pg/mL	1 pg/mL-100 pg/mL	[103]
alkylphenol	Anti- alkylphenol (adsorption)	Drop casted SWCNT, Si/SiO_2 substrate, Au electrodes (100 nm thick), IDE electrodes W/L (1.5/1000 µm), back-gated	Electrical measurement: I_{DS} vs [NP] Log ΔI_{NP} vs log NP	5 µg/L	5 µg/L-500 µg/L	[104]
Atrazine	anti-atrazine (adsorption)	Drop casted SWCNT, Si/SiO_2 substrate, Au IDE electrodes W/L (1.5/1000 mm), back-gated	Electrical measurement: ΔI vs log [ATZ]	0.001 ng/mL	0.001 ng/mL-10 ng/mL	[105]

Cathepsin E	Peptide aptamer (PBASE: Covalent binding)	CVD SWCNT, SiO_2/Si substrate, Ti/Au (2/40nm) electrodes, channel length 3 µm, liquid-gated	Electrical measurement: I_{DS} vs V_g $\Delta I/\Delta I_{max}$ vs [CatE]	2.3 pM (PBS) 0.23 nM (HS)	0.1 ng/mL-1 ng/mL (PBS) 10 ng/mL-100 ng/mL (HS)	[106]
TNF-α	Anti-TNF-α (EDS/NHS: Covalent binding)	SPM SWCNT, SiO_2 substrate, channel 3 µm in width and 300 µm in length, Pd/Au (10 nm/30 nm) metal electrodes, floating electrodes dimensions (15 µm × 300 µm), liquid-gated	Electrical measurement: I_{DS} vs V_g $\Delta G/\Delta G_{max}$/[TNF-α] I_{DS} vs Time	1 pg/L	100 fg/L-100 pg/L	[107]
GFP	VHH nanobody (EDS/NHS: Covalent binding)	Plasma torch SWCNTs diameter/length (0.9 –1.9 nm/0.3–4 µm), glass substrate, Cr/Au IDE bottom electrodes, channel W/L (2 mm, 20 µm), liquid-gated	Electrical measurement: I_{DS} vs $V_{Ag/AgCl}$ ΔV vs [GFP]	1 pM	1 pM-10 nM	[108]
DNA hybridization	DNA probe (PBASE: Covalent binding)	Suspended CNT, Si/SiO_2 substrate, Pd/Cr (100/3nm) electrodes, liquid-gated	Electrical measurement: I_{DS} vs V_{DS} I_{DS} vs V_g Resistance vs [DNA]	10 aM	10 aM-1 pM	[109]
cTnT	Biotinylated DNA aptamer (biotin-streptavidin chemistry)	Drop casted SWCNT + Au decorated-Co_3O_4, Si/SiO_2 substrate , IDE Ti/Au electrodes, distance between electrodes 100 µm, W of the device 24100 µm	Electrical measurement: I_D vs Time I_D vs [cTnT]	0.1 µg/mL 0.5 µA/µg.mL(S)	1µg/mL-10µg/mL	110]
Staphylococcus aureus	Polyclonal anti-Staphylococcus aureus (EDS/NHS: Covalent binding)	Alternating current dielectrophoresis SWCNT, Si/SiO_2 substrate, Cr/Au 10/100 nm Coplanar rectangular electrodes (gap/W: 20/50µm)	Conductance measurements	150 CFU/mL 2.95[%(log CFU/mL)] (S)	200-10^6 CFU/mL	[111]

COVID-19 (SARS-CoV-2)	RNA-dependent RNA polymerase gene of SARS-CoV-2	Simple process technique CNT, f lexible Kapton substrates, Cr/Au (5/50 nm) electrodes, liquid-gated	Electrical measurement: I_{DS} vs V_g $\Delta I/I$ vs [sequence]	10fM	10^{-6}nM-1 nM	[112]

ATZ: Atrazine: 2-chloro-4-ethylamino-6-isopropylamino-1,3,5-triazine; Au: gold; cTnT : cardiac troponin T; Cr: Chromium; DNA: Deoxyribonucleic acid; GFP : green fluorescent protein; HS: human serum; NP : 4-nonylphenol; IgG: Immunoglobulin G; Pd: palladium; PPy NT: polypyrrole nanotube; SWCNT: single walled carbon nanotubes; SPM: Standard photolithography method; Vg: gate voltage

Table 7. Graphene field-effect transistors for affinity sensing

Target	Receptor functionalization	FET Structure	Detection Technique	Detection limit (LOD)	Dynamic range	Ref
DNA	DNA probe (biotinylated BSA/streptavidin: adsorption)	CVD graphene transferred on 285-nm SiO_2 substrate, 15/200/7-nm-thick Cr/Au/Cr: source/ drain, liquid gated	Electrical measurement: I_{DS} vs V_{REF}	100 fM	-	[114]
22-mer miRNA	PNA probe (glutaraldehyde: covalent binding)	Au decorated RGO, SiO_2/Si substrate, liquid-gated	Electrical measurement: I_d vs V_g ΔV_{cnp} vs [miRNA]	1 fM	1 fM-100 pM	[115]
22-mer DNA	PNA probe (PBASE: Covalent binding)	PMMA transferred CVD graphene, Si O/Si substrate, Ti/Au electrodes, liquid-gated	Electrical measurement: I_d vs V_g ΔV_{dirac} vs [DNA]	1 fM	1 fM-100 pM	[116]
AFB1	anti-AFB1 antibody (PLL : adsorption)	RGO on the TCO coated glass substrate, Ag electrodes with a spacing of 0.8 cm,	Electrical measurement: I_{DS} vs V_{gs}	10^{-4} ppt in PBS	0.0001ppt-1ppt	

		5 mm by 5 mm, Gate platinum electrode 5 mm by 5 mm	Capacitance measurements	10^{-4} ppt in CS		[117]
IFN-γ	aptamer (adsorption)	PDMS transferred LPCVD Graphene, PDMS substrate, Ag electrodes, liquid gated	Electrical measurement: I_{DS} vs V_g Current at dirac point vs [IFN-γ]	83 pM	2 nM-100µM	[118]
Hep-B	anti Hep-B monoclonal antibody (glutaraldehyde: covalent binding)	EPD deposition of graphene bilayer on nanoporous SiO_2 substrate, IDE metal Ag/Au electrodes, liquid gated	Electrical measurement: I_{DS} vs V_{GS} I_{DS} vs time	0.05 fM	0.05 fM-1000 fM	[119]
SNP	double-stranded (DS) probes (PBASE: Covalent binding)	PMMA transferred CVD graphene, SiO_2/Si substrate, Ag electrodes, liquid gated	Electrical measurement: I_d vs V_g ΔV_{dirac} vs [SNP]	100 nM	100 nM-100 µM	[120]
DNA	DNA probe (PBASE: Covalent binding)	PMMA transferred CVD graphene, SiO_2/Si substrate, Cr/Au electrodes, back-gated	Electrical measurement: I_d vs V_g ΔV_{dirac} vs [DNA]	1 fM	10^{-18} M-10^{-4} M	[121]
CEA	Anti-CEA antibody (PBASE: Covalent binding)	PMMA transferred CVD graphene, SiO_2/Si substrate, Ti/Au electrodes, liquid-gated	Electrical measurement: I_{ds} vs time ΔI_{ds} vs [CEA]	100 pg/mL	100 pg/mL-100 ng/mL	[122]
20-mer DNA	PNA probe (PBASE: Covalent binding)	Wet method transferred CVD graphene, SiO_2/Si substrate, Cr/Au electrodes, liquid-gated	Electrical measurement: I_{ds} vs V_g ΔV_{cnp} vs Time ΔV_{cnp} vs [DNA]	10 pM	0.25 nM-10 nM	[123]
DNA	DNA probe (adsorption)	Transferred exfoliated graphene by adhesive tape on SiO_2/Si substrate, Ti/Au (10/200 nm) electrodes, liquid and back-gated	Electrical measurement: I_d vs V_{bias} I_d vs V_g	10 nM	10 nM-1000 nM	[124]

hCG	anti-hCG antibody (Pyr-NHS: covalent binding)	PMMA transferred CVD graphene, SiO_2/Si substrate, Au/Cr source/drain, SiO_2 300 nm and W, L of each FET 90 µm and 80 µm, back-gated	Electrical measurement: Resistance vs back gate voltage	1 pg/mL 0.30 Ω/ng ·mL (S)	1 pg/mL – 100 ng/mL	[125]
hCG	anti- hCG antibody (PBASE: covalent binding)	PMMA transferred CVD graphene on SiO_2 Substrate, Cr/Au electrodes, back-gated	Electrical measurement: I_{DS} vs V_g	6 pg/mL	1 pg/mL-100 ng/mL	[126]
HER2	Aptamer (PBASE: Covalent binding)	CVD graphene nanomesh transferred on meso-SiO_2 Substrate, flexible FETs, liquid gated	Electrical measurement: I_d vs V_d I_d vs V_g ΔI_d vs [HER2] ΔI_d vs time	0.6 10^{-15} M	0.0001 ng/mL-200 ng/mL	[127]
RNA	DNA probes (PBASE: covalent binding)	PMMA transferred CVD graphene on SiO_2/Si substrate, ITO electrodes Liquid-gated	Electrical measurement: I_{DS} vs Gate electrode I_{DS} vs V_g	0.1 fM	0.1 fM-1 pM	[128]
Cortisol	monoclonal cortisol antibody (Anti-Cab) (PBASE: covalent binding)	Graphene nanoplatelets 7 nm drop-coated on SiO_2/Si substrate, the L and W of the channel 500 µm x 1000 µm, electrolyte gated	Electrical measurement: I_{DS} vs V_{GS}	10 pg/mL	10 pg/mL – 10 µg/mL	[129]
OA	anti OA (adsorption)	Graphene nanoplatelets drop-coated on SiO_2/Si substrate, interdigitated electrodes of 1.5 µm of W and 1000 µm of L, back-gated	Electrical measurement: I_{DS} vs V_{DS}	0.05 ng/mL	0.05- 300 ng/mL	[130]
Hep-B	anti-Hep-B antibody (glutaraldehyde: covalent binding)	Graphene solution deposited on NPSO substrate, IDE metal electrodes width 60 µm and spaced with 60 µm	Electrical measurement: I_D vs V_{GS}	0.1 fM	0.1 fM -1 pM	[131]

			C_T vs Frequency			
hCG	anti- hCG antibody (Pyr-NHS: covalent binding)	CVD graphene on SiO_2/Si substrate, Cr/Au electrodes, channel length 720 µm, width of GFET channels 80 µm, back-gated	Electrical measurement: I_{DS} vs V_{DS} Resistance vs [hCG]	1 pg/mL	1 pg/mL - 1 ng/mL	[132]
CA 125	anti-CA125 ssDNA (CMWCNT/EDC/NHS : covalent binding)	CNT + RGO, PMMA substrate, Flexible FET Au electrodes (W= 5 mm and L = 1 mm channel) gate electrode Pt, liquid gated	Electrical measurement: I_d vs V_g	5 10^{-10} U/mL	10^{-9}-1 U/mL	[133]
AFP	anti- AFP antibody (PBASE: covalent binding)	CVD graphene transferred on PET substrate Au 10 nm electrodes, gate channel size W= 5 mm and L= 500 µm, electrolyte gate	Electrical measurement: I_{ds} vs V_{gs} I_{ds} vs V_{ds} ΔV_{dirac} vs [AFP]	0.1 ng/mL (PBS) 16.91 mV (S) 12.9 ng/mL (HCCPP) 5.68 mV (S)	0.1 ng-250 ng/mL (PBS) 12.6 ng/mL-784.9 ng/mL (HS)	[134]
TSH	anti-TSH $F(ab')_2$ (PBA/EDC/NHS: covalent binding)	PMMA transferred CVD graphene on glass substrate, Au electrodes channel W ≈ 3 mm, L ≈ 0.75 mm, electrolyte gated	Electrical measurement: G_s vs V_g ΔV_g vs [TSH]	0.2 10^{-15} M 10x10^{-15} M (S)	10^{-14}M-10^{-8} M	[135]
SNP	DNA probe (PBASE: covalent binding)	PMMA transferred CVD graphene on SiO_2/Si substrate, Cr/Au (3/30 nm) electrodes, electrolyte gated	Electrical measurement: ΔV_{dirac} vs [SNP]	25 aM 24 mV/dec (S)	1 aM-100 pM	[136]
Single-Strand DNA	aptamer (PBASE: covalent binding)	Transferred CVD graphene, glass substrate, ITO electrodes, back-gated	Impedance: Impedance Change of MGFET vs MFI/Time/[DNA]	1 pM	1 pM-10 nM	[137]

chlorpyrifos	Anti-chlorpyrifos antibodies (EDC/NHS: covalent binding)	Exfoliated graphene transferred by scotch tape on 285 nm SiO_2/Si substrate, Cr/Au (5/50nm) electrodes, back- gated	Electrical transport: Resistance vs V_g/time	1.8 fM	1 fM-1µM	[138]
CTn1	anti-CTn1 antibody (EDC/NHS: covalent binding)	PMMA transferred exfoliated graphene on 285 nm SiO_2/Si substrate, Cr/Au (5/50 nm), back-gated	Electrical measurement: Resistance vs V_g/Time Current vs time	10 fg/mL	1 fg/mL- 1 µg/mL	[139]
CCP	anti- Cyclic citrullinated peptide antibody (EDC/NHS: covalent binding)			10 fg/mL		
P24	anti-P24 antibody (EDC/NHS: covalent binding)			100 fg/mL		
Exosomes	anti-CD63 antibody (PBASE: covalent binding)	PMMA transferred CVD graphene on SiO_2/Si Substrate Ti/Au electrodes, back-gated	Electrical measurement: I_{ds} vs V_g I_{ds} vs V_{ds}	0.1 µg/mL	0.1µg/mL-10 µg/mL	[140]
DNA (bfp)	Cas9-sgRNA (dRNP) (complexation)	Graphene tranferred on SiO_2/Si Substrate Ti/Pt electrodes	Electrical measurement: I vs time I vs [DNA sample] I vs [HEK DNA]	2.3 fM 1.7 FM (S)	-	[141]
COVID-19 (SARS-COV-2)	SARS-CoV-2 spike protein antibody (PBASE: covalent binding)	PMMA transferred Graphene on a SiO_2/Si substrate, Au/Cr electrode L x W (100 x 100 μm^2), electrolyte gated	Electrical measurement: I_{DS} vs V_{DS} I_{DS} vs V_{GS} $\Delta I/I_0$ vs time	$1.6x10^1$ pfu/mL (CM) $2.42x10^2$copies/mL (CS)	$1.6x10^1$ -$1.6x\ 10^4$ pfu/mL	[3]

7 amino acids (BGP-C7)	antibody variable fragment V_L (PBASE: covalent binding)	Graphene transferred on SiO_2/Si substrate, Au electrodes, electrolyte-gated	Electrical measurement: $\Delta I_d/g_m$ vs Time $\Delta I_d/g_m$ vs [BGP-C7]	10 fg/mL	10 fg/mL-1000 ng/mL	[142]
Hep-B	anti-Hepatitis-B monoclonal antibody (EDC/NHS: covalent binding)	ERGO on FTO coated glass substrate, electrolyte-gated	Electrical measurement: I_{mix} vs frequency I_{mix} vs V_g I_{mix} vs time	1 fM	1 fM - 100 fM	[143]
AFP	anti- AFP antibody (adsorption)	GO nanosheets deposited on SiO_2/Si substrate, Au/HRE-RGO electrodes	Electrical measurement: I_{DS} vs V_g	-	-	[144]
Biotin	Avidin (PBASE: covalent binding)	PMMA transferred CVD graphene on SiO_2/Si substrate, Cr/Au (100 nm) IDE electrodes, Electrode W= 200 µm, gap between the electrodes=200 µm, electrolyte gated	Electrical measurement: I_{DS} vs time I_{DS} vs [Biotin] I_{DS} vs V_{gs}	90 fg/mL	90 fg/mL -9.33 ng/mL (0.37pM)	[145]
Nucleic acids	DNA probe (PBASE: covalent binding)	PMMA transferred CVD graphene on a polystyrene substrate, Ag electrodes, back-gated	Electrical measurement: I_{DS} vs V_{gs}	600 zM (PBS) 20 aM (HS)	600 zM-60nM (PBS) 20 aM-200 fM (HS)	[146]
Clusterin	anti-clusterin antibody	Graphene transferred on SiO_2/Si substrate, Cr/Au electrodes	Electrical measurement	1 pg/mL	1 pg/mL - 1 ng/mL	[147]
JEV	Monoclonal antibodies JEV (EDC/NHS: covalent binding)		Electrical measurement:	1 fM	1 fM -1µM	

AIV	Monoclonal antibodies AIV (EDC/NHS: covalent binding)	Exfoliated graphene with scotch tape, SiO_2/Si substrate, Cr/Au (5/50 nm) electrodes, back-gated	Resistance vs V_g	10 fM		[148]
COVID-19 (SARS-COV-2)	SARS-CoV-2 spike protein antibody (PBASE: covalent binding)	-	-	1 fg/mL		[149]
DNA hybridization	probe DNA (PBASE: covalent binding)	PMMA transferred CVD graphene on SiO_2/Si substrate, ITO electrodes with the area of sensing channel of 1 cm × 0.4 mm, liquid gated	Electrical measurement: I_{DS} vs V_g I_{DS} vs V_{ds}	10 aM	10 aM-100 fM	[150]
Cortisol	Mouse monoclonal cortisol antibody (PBASE: covalent binding)	Graphene nanoplatelets dispersion drop-casted on SiO_2/Si substrate, Ni/Au (300 nm) electrodes, dimension of the device L x W (2.0 cm x 0.5 cm), electrolyte gated	Electrical measurement: I_{DS} vs V_{GS} ΔV_{GS} vs [Cortisol]	0.85 pg/mL 72.30 µA/g.mL (S)	1 pg/mL-10 ng/mL	[151]
DNA	PNA probes (PBASE: covalent binding)	Drop casted graphene ink on PCB, Ag electrodes W/L (0.13/5 mm), electrolyte-gated	Electrical measurement: I_{DS} vs V_g	1 nM 30.1 mV/dec (S)	0.1 nM-1000 nM	[152]
PSA	anti-PSA antibodies (glutaraldehyde: covalent binding)	DEP deposition of RGO, SiO_2/Si substrate, (Cr/Au) Electrodes, W/L (50/500 µm), gap between electrodes (100 µm) and height is 4 mm, electrolyte-gated	Electrical measurement: I_{mix} vs V_{GS} I_{mix} vs Time G vs [PSA]	1 pg/mL	1 pg/mL-4 ng/mL	[153]

COVID-19 (SARS-COV-2)	complementary phosphorodiamidate morpholino oligos (PMO) probe (EDC/NHS: covalent binding)	RGO drop-casted on 285 nm SiO_2/Si substrate, Au electrodes (50 nm thick), liquid gated	Electrical measurement: I_{DS} vs V_g/ Time ΔV vs [SARS-COV-2]	PBS 0.37 fM TS 2.29 fM serum 3.99 fM	1 fM-1pM	[154]
Geosmin	Geosmin aptamer (bioprobe) (PDI-diacid/DMTMM: covalent binding)	Wet-transferred CVD graphene on SiO_2/Si substrate, Cr/Au (1:10 thickness ratio; Cr 10 nm/Au 100 nm) electrodes, liquid-gated	Electrical measurement: I_{DS} vs V_g	0.01 nM	0.01 nM-1 µM	[155]
HPV-16 E7 protein	aptamer (EDC/NHS: covalent binding)	RGO transferred on IDE Au electrodes, glass substrate, Liquid-gated	Electrical measurement: ΔI_{DS} vs V_g/ Time	100 pg/mL (1.75 nM)	30 nM- 1000 nM	[156]
LMW imatinib	Abl1 protein (PBASE: covalent binding)	Wet-transferred CVD graphene on SiO_2/Si substrate, nm Cr/ Au (20/100 nm) electrodes, graphene channels L/W (45/45 µm), PMMA microfluidic channel L/W (10/0.5 mm)	Electrical measurement: I_{DS} vs V_{gs} I_{DS} vs concentration I_{DS} vs Time	15.5 fM	0.1 pM- 10 µM 0.0194 µA/fM (S)	[157]
BNP	BNP antibody (50E1 antibody) (adsorption)	B/N co-doped GO spin-coated on SiO_2/Si substrate, Au/Ti electrodes, back-gated	Electrical measurement: I_{DS} vs V_g	10 aM	10 aM- 1µM	[158]
Single-stranded DNA	DNA probe (PBASE: covalent binding)	Optic-fiber GFET, wet-transferred CVD graphene on quartz fiber, Au electrodes, liquid gated	Electrical measurement: Current of OGFET vs V_g/time	10 nM	10 nM-500 nM	[159]
Exosomes	anti-CD63 Antibody (PBASE: covalent binding)	CD modified PMMA transferred CVD graphene on SiO_2/Si substrate, Ti/Au	Electrical measurement: I_{DS} vs V_{GS}	100 particles/µL	10-10^7 particles/µL	[160]

		(10/50 nm) electrodes, PDMS channel L/W(6/0.5 mm), liquid-gated	ΔV_{DV} vs [Exosome]			
Clusterin	anti-clusterin antibody (Pyr-NHS: covalent binding)	Transferred CVD graphene on SiO_2/Si substrate, Cr/Au electrodes, back-gated	Electrical measurement: Current vs voltage/ back voltage	300 fg/mL (4 fM)	1pg/mL-100 pg/mL	[161]
IFN-γ	IFN-γ-specific aptamer (adsoption)	Wet-transferred CVD graphene, 285 nm SiO_2/Si substrate, Cr/Au (2/43 nm) electrodes, electrolyte-gated	Electrical measurement: I_{DS} vs Vg ΔV_{dirac}/ $\Delta V_{dirac,max}$ vs [IFN-γ]	740 fM	0.015nM-250nM	[162]
DNA	Cas9	Bubble transferred CVD Graphene on SiO_2/Si Substrate Ti/Pt electrodes	Electrical measurement: $C_{response}$ vs Time/[DNA]		10-60 ng/µL	[163]
Cortisol	Aptamer (61 basepair) (PBASE: covalent binding)	graphene FET, Pt extended gate functionalized with a single graphene layer	Electrical measurement: I_{DS} vs V_{REF} VREF vs [cortisol] S_I vs [Cortisol]	0.2 nM	1 nM-10 µM	[164]

AFB1: Aflatoxin B1; AFP: α-fetoprotein; AIV: Avian Influenza Virus; Au: gold; Ag: Silver; BGP-C7: C-terminal 7-mer peptide of human osteocalcin bone gla protein; CA 125: Ovarian cancer antigen; CCP: Cyclic citrullinated peptide; CTn1: Cardiac troponin 1; CEA: carcinoembryonic antigen; Cr: Chromium; CM: culture medium; CS: clinical sample; cnp: charge neutrality point voltages; C_T: total capacitance; CS: corn samples; CMWCNT: carboxylated multiwalled carbon nanotubes; CVD: chemical vapor deposition; Cu: Copper; DNA: Deoxyribonucleic acid; ERGO: electrochemically reduced graphene oxide; FET: Field Effect transistor; FTO: fluorine doped tin oxide, DMTMM: 4-(4,6-Dimethoxy-1,3,5-triazin-2-yl)-4-methylmorpholinium chloride; g_m: Transconductance; G : Conductivity; hCG: Human Chorionic Gonadotrophin; HER2: Human epidermal growth factor receptor 2; Hep-B: Hepatitis-B; HRE- HPV: human papillomavirus; HS: human serum; HCCPP: Hepatocellular carcinoma patient plasma; HCG: human chorionic gonatrophin; I_{mix} : mixing current; IDE : Intergitated electrodes; I_{DS}: Drain current; IFN-γ: Interferon gamma; ITO: indium tin oxide; JEV: Japanese Encephalitis virus; L: length; LPCVD: low pressure chemical vapor deposition; LMW: Low molecular weights; MFI: Magnetic Field Intensity; MGFET: Magnetic graphene Field Effect transistor; NPs: nanoparticles; NPSO: nanoporous silicon

oxide; OA: Okdaic acid; OGFET: optic-fiber graphene field effect transistor; PMMA: polymethyl methacrylate; PSA : prostate specific antigen; PNA : peptide nucleic acid; PDMS: polydimethylsiloxane; PBASE: 1-pyrenebutanoic acid succinimidyl ester; PBA: pyrenebutytic acid; PDI-diacid: bis(2-aminoethylene) perylene-3,4,9,10-tetracarboxyldiimide; PDMS: Polydimethylsiloxane; Pt: platinum; PLL: poly-L-lysine; RGO: higher reduction extent- reduced graphene oxide; TCO: transparent conductive oxide; TSH: thyroid stimulating hormone; Ti: titanium; TS: throat swab; SNP: Single-nucleotide polymorphisms; S: sensitivity; Si: Silicon; SiO_2: Silicon oxide; Vg: gate voltage; V_{ds}: Drain to source voltage; W: width.